RSC Advances

ROYAL SOCIETY OF CHEMISTRY

www.rsc.org/advances

Cite this: DOI: 10.1039/c0xx00000x

www.rsc.org/xxxxxx

ARTICLE TYPE

A Review of Structure of Oxide Glasses by Raman Spectroscopy

Avadhesh Kumar Yadav,*[a] and Prabhakar Singh[a]

[a]*Department of Physics, Indian Institute of Technology (Banaras Hindu University), Varanasi-221005 (India)*

**E-mail: yadav.av11@gmail.com*

The family of oxide glasses is very wide and it is continuously developing. The rapid development of advanced and innovative glasses is under progress. The oxide glasses have variety of applications in the daily use articles as well as advanced technological fields like protection of X-ray, fibre, optical instruments or lab glasswares. The oxide glasses are basically consisted by network formers such as borate, silicate, phosphate, borosilicate, borophosphate and network modifiers like alkali, alkaline earth and transition metals. In present review article, Raman spectroscopic results for structures of borate, silicate, phosphate, borosilicate, borophosphate, aluminosilicate, phosphosilicate, alumino-borosilicate and tellurite glasses are summarized.

1. Introduction

1.1 Brief history of glass

The exact history of glass is not known but there are certain evidences which confirm that it is used about 3500 BCE in Mesopotamia. The available archaeological evidence gives the signature of presence glass articles in coastal north Syria, Mesopotamia or Ancient Egypt. The glass technology in South Asia was started with 1730 BCE [1]. The evidences of glass have also been found in Hastinapur and archaeological site in Takshashila, ancient India. The glass objects have been developed in Romanian Empire and Anglo-Saxon period in domestic, industrial and funerary contexts. In china, the development of glass was started late but nowadays, glass played a peripheral role in arts and crafts. The glasses from that period are made of barium oxide (BaO) and lead [2]. The tradition of use of the lead-barium glasses was disappeared at the end of the Han Dynasty (AD 220). The soda glasses with high alumina are rarely used around the Mediterranean area or in the Middle East. The soda-lime, borosilicate, glass fibre, lead, alkali-barium silicate, aluminosilicate, vitreous silica and pyrex glasses were investigated time to time. The large scale development glass technology was started mainly from 14th century [3]. The recent research on glasses are based on advanced glasses used for safety systems like X-ray protective glasses, fibre glasses, high refractive index glasses for optical instruments, photo-chromatic and high strength glasses.

Last few decades, the oxide glasses have attracted the attention of researchers and scientist due to their extensive properties which are very useful for many applications. They are easily shaped due to lack of underlying crystal structure. The covers of solar units and photovoltaic units improve the performance. In turbines, glass fibers reinforced composites are used for the purpose of storage of wind energy. For this purpose, boron-free glasses are commonly used [4]. The oxide glasses may be used in smaller power supplies, including dielectrics for super-capacitors, sealants for high-temperature solid oxide fuel cells (SOFC) and electrolytes for electrochemical devices [5]. W. H. Zachariasen had investigated the silicate glasses and he found that such glasses are consist of silicon tetrahedrally coordinated to 4 oxygen atoms [6]. The phosphate glasses are investigated P. B. Price et al [7]. Borate glasses have been investigated in various glass systems B_2O_3-xLi_2O_3 [8], xB_2O_3-(1-x)Li_2O_3 [9-10], (30 - x)Li_2O - xK_2O - 10CdO/ZnO - 59B_2O_3 [11], 60B_2O_3–(20-x)Na_2O–10PbO–10Al_2O_3:xTiO_2:yNd_2O_3 [12], PbO-Bi_2O_3-B_2O_3 [13], Bi_2O_3-B_2O_3-ZnO-Li_2O [14], Gd_2O_3–MoO_3–B_2O_3 [15]. The silicate glasses were investigated in presence of Na_2O, Li_2O, K_2O and CaO by various research groups [16-25]. The phosphate glasses are investigated for long time in many systems. The calcium, sodium, potassium, iron, gadolium, zinc, lead, chromium, molybdenum, lanthanum, bismuth, tungsten, samarium, copper, cadmimium, barium, silver contained phosphate glasses have been investigated for various application purpose [122-165]. Soon after single network former glasses, double network former glasses have also been investigated for composite network structure of borate, silicate and phosphate which are named as borosilicate, borophasphate etc glasses. In recent years, the structure properties of SnF_2–SnO–P_2O_5 glasses have been studied. In this study, the glass transition temperature was found to be very low [26]. CeO_2 in cerium iron borophosphate glasses increases the glass transition temperature and also increases thermal stability [27]. The thermal stability of Na_2O–FeO–Fe_2O_3–P_2O_5 was found to be poorer than sodium-free iron phosphate glasses [28]. TiO_2 is useful for increasing the thermal stability of BaO–Li_2O–diborate glasses [29]. The low melting glasses were prepared in the glass system K_2O–MgO–Al_2O_3–SiO_2 [30]. For the purpose of immobilisation of nuclear waste, few borosilicate glass were also investigated in glass system 55 SiO_2–15 B_2O_3–5 Al_2O_3–5 CaO–(20–x)Na_2O–xCs_2O [31].

Glass may be defined as inorganic solids, which are amorphous in nature. They are classified in several groups like

metallic alloys, ionic melts, aqueous solutions, molecular liquids and polymers. They have attracted the attention of researchers and scientists in recent years due to demand in many significant applications like fields of energy science and photonics. The substantial growth of glasses is still required.

1.2 Brief Chemistry and Physics of Glasses

Glasses are disordered materials i.e. lack of the periodicity in crystal structure [32] and are formed by cooling of melt of inorganic products to rigid condition without crystallization [33-34]. Several materials like organic polymers and metal alloys have also amorphous structures but all of them are not glasses [35]. The formation of glass requires critical cooling rates [36-39]. Thermodynamically, the glasses are non-equilibrium materials because their properties are the function of pressure, temperature and composition. They are always approached to its nearby metastable state [40-43]. Glass formation is possible if glass composition contains network formers. They are formed by the network formers such as borate, silicate, phosphate, borosilicate, borophosphate etc. It is found that the excellent glass formers have electro-negativity values of 1.7–2.1 on the Pauling scale [44]. The sufficient network modifiers are used in glass formation to modify the glass properties. The glass network is modified by alkali and alkaline earth metal modifiers like ZnO, PbO, TeO_2, Bi_2O_3, MgO, CaO, SrO, BaO, CeO_2, Cr_2O_3, La_2O_3, CdO, CuO, Li_2O, Na_2O, K_2O, Al_2O_3, MgF_2 etc. The alkali ions are easily thermally activated which can move from one site to another within a glass. This type of movement of alkali ions within a glass structure enables to replace alkali ions near the surface of glass by other ions of the same valence [45-46]. Several local packing arrangements are available in glasses which enable the tuning of their properties through composition and processing. This permits creation of highly homogeneous materials on a macroscopic scale [47]. Zachariasen establish a theory which explains the criteria for vitreous structures with highly directed three-dimensional bond arrays. The glass structures are comprised of microcrystallites ~ 20 Å in size. The glass structures lie between a melt state and a glassy state [48-49]. The glassy network structure may be effectively understood by infrared and Raman spectroscopy. Certain viscosity models are used to explain the glass properties on temperature scale. The five temperatures named as standard points (associated with the viscous flow of glass), strain point (maximum temperature supported by glass), annealing point (relieve the internal stresses), softening point and working point (most glass forming operation acting at this temperature) [50].

1.2.1 Classification of Preparation Method of Glasses

The glasses are mainly synthesized by melt-quenched method, sol-gel method and chemical vapour deposition [51].

1.2.1.1 Glass by Melt-Quench Technique

The melt-quench technique is the first discovered technique for preparation of glasses. In melt quench method, the inorganic raw materials are properly weighed according to composition. Then, the raw materials are mixed properly in mortar with pestle or ball mill in acetone media. The well mixed and dried ingredients are placed into high grade alumina or platinum crucible and crucible is place in programmable temperature controlled furnace for melting. The homogonous melt is quenched in aluminium mould. In this way, the glass is formed by melt quench method. Formed glasses are annealed at relatively low temperature to the glass casting temperature to remove the residual internal stresses which are produced due to temperature gradient during forming and subsequent cooling [52]. The melt quench method is advantageous for obtaining materials of large size compared to single crystal or polycrystalline ceramics. It has one more advantage that it provides large flexibility of composition over chemical vapour deposition or sol-gel method. This method has also certain disadvantages. For example, this method is not good for preparation of glasses of ultra-high purity which are used in optical communication. Certain contamination and impurity of crucible or furnace materials is also added in the glass in this method. Glasses, in which refractory materials like SiO_2, TiO_2, Al_2O_3, ZrO_2 etc are used, are difficult to prepared by this method due requirement of extremely high temperature.

1.2.1.2 Glass by Sol-gel Method

In sol-gel method, the colloidal solution (sol) of raw materials is converted into gelatinous substance (gel). In this method, there is no requirement of any melting and quenching. The fine-grained gel bulks of various organic compounds are annealed at particular temperature and thereafter the annealed gel was sintered at higher temperature than the annealing temperature. During this process, there are two reactions take place, named as hydrolysis and condensation reaction [53].

1.2.1.3 Glass by Chemical Vapour Deposition Method

The chemical vapour deposition (CVD) method for preparation of bulk glasses was developed in the early 1940. For the formation of glass material is followed by thermally activated homogeneous oxidation or hydrolysis of the initial metal halide vapour. The oxidation or hydrolysis reaction is activated by an oxy-hydrogen flame or oxygen plasma. In this method, the initial components are liquid at room temperature and their boiling temperature is very low compared with halides of alkali, alkaline earth, transitions metals or rare- earth elements. The purification of raw materials is done by repeating the distillation bellow melting points. This method is advantageous for preparation of ultra-high purity glasses [54].

The structural study of glass networks is important for understanding the composition dependence of oxide glass properties. Various models are proposed for correlating the different properties with structure and composition of glassy system. Phillips and Thorpe investigated the compositional dependence of glass properties by analyzing the topology of the glassy network. This approach is based on the comparison of the number of atomic degrees of freedom with the number of interatomic force field constraints. The tendency for glass formation would be maximized if the number of degrees of freedom exactly equals the number of constraints in the glassy network [55]. Gupta and Mauro have demonstrated generalization of the Phillips and Thorpe approach in their study [56, 253].

This review article is focused on the structural study of various oxide glasses and how the structure of glassy network is modified by various dopants like alkali, alkaline and transitions metals. The compositional dependent study of oxide glasses are also summarized in present review article. This review article is very useful for understanding the formation of glassy networks and their modification by various dopants.

1.3 Brief Introduction to Glassy Networks

A lot of work has been done glassy materials till now. The glassy materials consist of various network former like borate, silicate, phosphate, borosilicate, borophosphate etc. The borate network consists of vibrations of isolated diborate ($B_4O_7^{2-}$) groups, breathing of O-atoms, loose diborate vibrations, chain or ring type meta- and pentaborate ($B_5O_8^-$) groups, symmetric breathing vibrations of six member borate rings with one or two BO_3 triangle replaced by a (BO_4^-) tetrahedral, symmetric breathing vibrations of boroxol rings, triborate ($B_3O_5^-$), terta-borate ($B_8O_{13}^{2-}$), ortho-borate (BO_3^{3-}), pyro-borate ($B_2O_5^{4-}$) groups, linked $[BO_3]^{3-}$ triangles with one free vertex etc [45, 57]. The borate glasses have significant importance in several applications in thin amorphous films for battery application, bioactive glasses for tissue engineering, nuclear waste disposals, photonic applications, development of tuneable or short pulse lasers, optical fibre amplifiers and fibre lasers [58-61]. The borate networks are shown in Fig. 1.

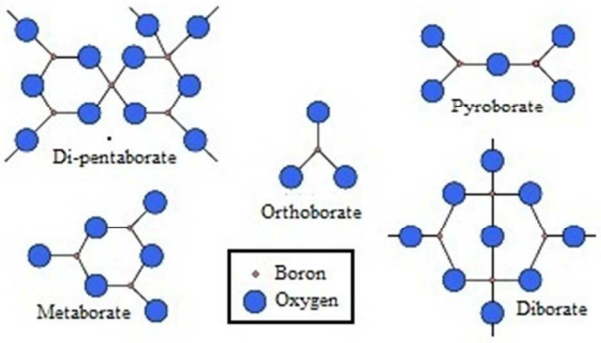

Fig. 1: The network units of borate glasses [107]. (Reproduced with permission of IOP Publishing)

The silicate network former is also significant for glass formation but the silica is not easily fusible and has not retained viscosity for long time. Thus, it cannot form the glass easily. Certain substances are used which help in the formation of glassy network, called fluxes [62]. The silicate glasses consist of tetrahedral 6-coordinated 4 oxygen atoms. 6-coordinated silicon is also found in few crystalline materials [63]. The silicate networks are found in the form of structural units of orthosilicate, Si - O stretching vibrations of tetrahedral silicate units, symmetric stretching vibrations of silicate tetrahedra, inter-tetrahedral Si - O - Si linkages and structural unit Q_{Si}^n (n = 0 to 4), where, Q_{Si} represents the tetrahedral unit and n is the number of bridging oxygen (BO) per tetrahedron [64-66]. Silicate glasses are, generally, used for application of windows, lenses, mirror substrates, crucibles, trays and boats, UV transmitting optics (synthetic fused silica), IR transmitting optics and metrology components. The network units of silicate glasses are shown in Fig. 2. Alike to silicate network, phosphate network is formed by various structural units of phosphate. The phosphate glasses are formed at low temperature in comparison to silicate glasses. The vibrational units of phosphate networks are Q_P^n groups of PO_4 tetrahedra (n = number of bridging oxygen per PO_4 tetrahedron), symmetric stretching of P - O, asymmetric stretching vibration of P - O, P - O - P symmetric vibrations, bending vibrations of phosphate polyhedra and O - P - O bending modes. The phosphate glasses have numerous applications in photonics, biomedical applications, solid state electrolytes, fibres etc [67-69]. The phosphate glasses are much sensitive in ionizing particles. This property of phosphate glasses enables the use for identification of heavy ions [70]. The phosphate networks are shown in Fig. 3.

Not only single network former glasses were performed but also double network former glasses were also investigated. The borosilicate glasses are one of the double network former glasses. The co-existence of borate and silicate networks is associated in borosilicate glasses. The interlinking of some borate and silicate networks is also possible in such glasses. The high frequency band > 850 cm^{-1} are related with silicate networks, Q_{Si}^n, whereas mid frequency bands (400 to 850 cm^{-1}) are order superstructures, reedmergnerite $[BSi_3O_8]^-$ and danburite $[B_2Si_2O_8]^{2-}$. The bands ranges between 300-500 cm^{-1} are the characteristic of mixed stretching and bending modes of Si-O-Si units while bands in the range 550-850 cm^{-1} are caused by ring breathing modes. The bands at 670, 770 and 808 cm^{-1} are the signature of tetraborate groups, four- and three-coordinated boron in diborate and boroxol rings, respectively. The borosilicate glasses are mainly used in lab equipments, high quality medical devices (ampoules, dental cartridges, veterinary tracking devices etc), space exploration devices and electronics (microelectromechanical systems) [71-74].

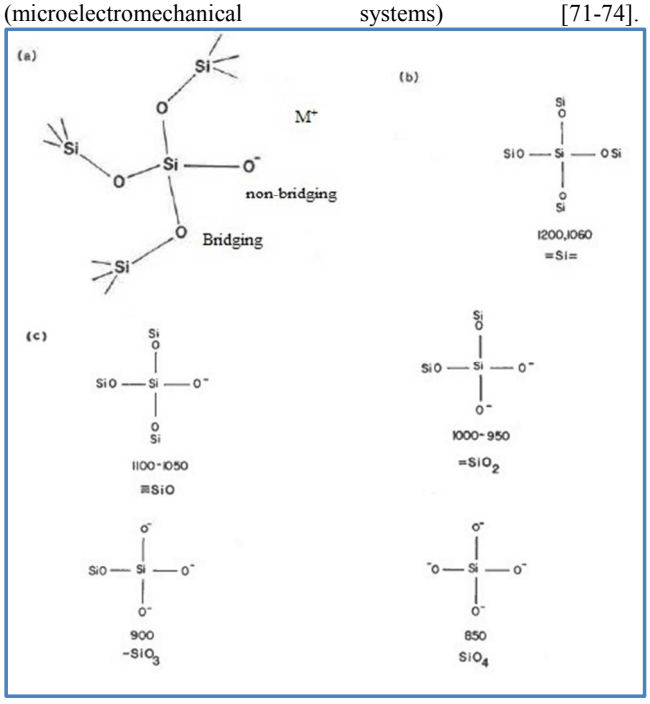

Fig. 2: The network units of silicate glasses [16]. (Reproduced with permission of Mineralogical Society of America)

Borate has an ability to change their properties and control them by a suitable modification of their chemical compositions within a relatively broad concentration region of their constituents in phosphate glasses. Addition of borate (B_2O_3) to phosphate glasses improves their mechanical properties and chemical resistance against atmospheric moisture. The borophosphate glasses includes the networks of both borate and phosphate alongwith various linking vibrations. These glasses are very useful for potential applications in solid electrolytes, glass solders and glass seals [75-76]. Phosphosilicate glasses consist of networks of phosphate as well as silicate. The phosphosilicate glasses are used in forming the Raman fibres laser and amplifiers. Phosphosilicate

glasses are useful in developing high refractive index grating [77-78]. Aluminosilicate glasses contain the units of silicate and aluminate networks. These are very important for geological applications due to its highly refractory nature [79-80]. The aluminium based glasses have a great technological importance due to their strong and ductile nature. These play an important role where metallic glasses failed [81]. Alumino-borosilicate glasses are formed by the networks of aluminate, borate and silicate. These glasses have wide range of applications in optical, thermal, electrical and mechanical properties. Along with these properties, the addition of Al_2O_3 to borosilicate matrix improves the chemical durability, decreases thermal expansion coefficient, electrical even radiation resistant and widens the scope of applications of borosilicate glasses [50]. The doping of alkali and alkaline earth metals in these glasses modified the parent network. Rare-earth ion-doped glasses have importance in application like optical fibre lasers, amplifiers and scintillating glasses. Sm^{2+} doped glasses are advantageous for spectral hole burning [83-88].

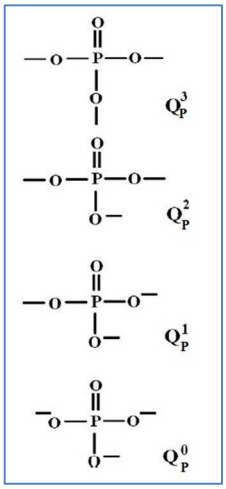

Fig. 3: Network units of phosphate glasses [164]. (Reproduced with permission of Elsevier)

2. Principle of Raman spectroscopy

Raman spectroscopy is a powerful tool for structural analysis and developed by Sir C. V. Raman and Kirishnan in 1928 [89]. They pointed in their study that Raman intensity is 10^{-6} to 10^{-9} times less to Rayleigh scattering. Such low intensity can be produced by lasers [90]. When a laser light is incident on vibrating molecules, then, the energy of photon may be changed. The exited molecule or atoms return to different states. The change in energy between the original state and the new state gives shift of emitted photon. The excited molecule goes to higher or lower frequency side to original state and referred as Stoke Raman scattering, (Stoke shift) or anti-Stoke Raman scattering (anti-Stoke shift), respectively [91-92]. The detailed description of working principle is shown in Fig. 4. The chemical composition and structure of molecules influence the modified scattering and no two of the spectra being exactly similar. Thus, Raman shift may be useful in distinguishing structure of different constituents and molecules [93-94].

Raman spectroscopy is used for determination of the structure, environment and dynamics of glassy materials. Furthermore, the portability of the technique allows for its use in on-line process monitoring over other instruments like Infrared spectroscopy,

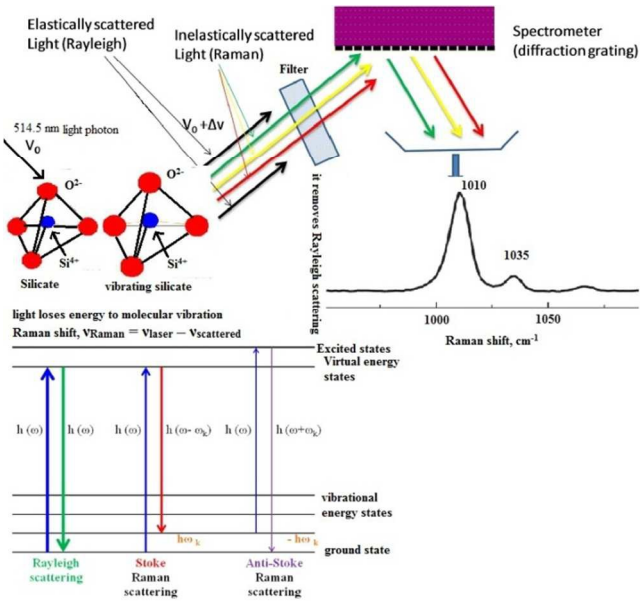

Fig. 4: Working principle of Raman spectroscopy

NMR and X-ray diffraction techniques [95]. Raman and infrared (IR) spectroscopy are used as complimentary techniques and both techniques differ slightly by their selection rule. IR spectra arise from a change in the dipole moment whereas Raman bands arise from a change in the polarizability. Few transitions are allowed in Raman spectroscopy but forbidden in IR spectra, so Raman spectroscopy gives the significant information in that situation. Similar to Raman spectroscopy, in FT-IR spectrometer of UV-is spectrometer, the characteristics of sample are analysed by the absorbance (or transmission) spectrum. In IR spectroscopy, molecules like water or acetone are strong IR absorbers whereas sodium chloride or potassium bromide is very less significant absorbers (window materials). Thus, the functional groups such as hydroxyl or carbonyl are easily detected whereas window materials are not easily detected. However, the situation is different for Raman spectroscopy. In Raman spectra, the ordinate axis normally has arbitrary rather than absorption or %T units because it is simply a measure of the number of scattered photon counts captured by the detector at any particular frequency. If the power of incident laser on the sample is varied, then, the intensity of the Raman spectrum will vary accordingly. Therefore, the peak height in a Raman spectrum is not simply a function of the sample thickness which is different for IR spectrum which depends on sample thickness.

In UV/Visible and IR spectroscopy, the spectral contribution from the instrument is removed by using a reference beam or by subtracting a background spectrum. However, in Raman spectroscopy, any contribution or variation due to the instrument is considered a single-beam is used in it. Due to this reason Raman spectroscopy is play a vital role for quantitative analyses. Thus, the unwanted contributions can be minimized by Raman spectroscopy.

X-ray fluorescence (XRF) is also useful for elemental analysis

of glassy network whereas the vibrational networks cannot understand significantly by XRF. One more thing, a very high energy is required for its operation. X-ray powder diffraction method is also used for understanding the nature of glassy materials but this method is not much useful for network analysis of glassy material [96-98].

3. Discussion

3.1. Borate Glasses

A typical Raman spectrum of lithium borate glass is shown in Fig. 5 [99]. Raman study of lithium borate glasses depicts the networks of $B_{(4)}$ - O vibration of tetracoordinated boron at 520.5, 769 and 784 cm^{-1}, the vibrations of $B_5O_8(OH)_4$ units at the 555.5 cm^{-1} and the vibrations of tricoordinated boron near 919 cm^{-1}. The characteristics intense peaks at 500.5 and 884.5 cm^{-1} correspond to the vibrations of $B_{(3)}$-O in $B(OH_3)$. The sol-derived borate glasses show the presence of boroxol ring as band is found at 807 cm^{-1} [99].

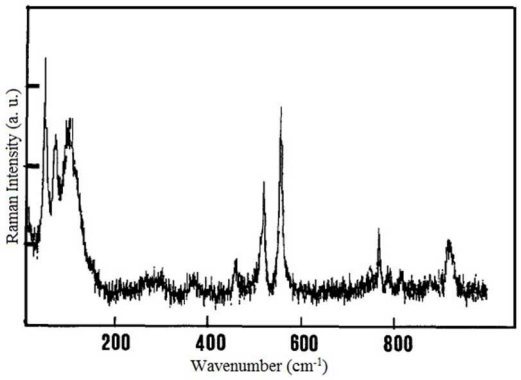

Fig. 5: Raman spectrum of lithium borate glass [99] (Reproduced with permission of Springer)

The Li cations are found in two distinct mode as non-bridging oxygen (NBO) type and bridging oxygen (BO) type sites. The primary network is formed by NBO and BO atoms in tetrahedral borate units, which reside close to NBO atoms. They modify the network by making cluster around NBO atoms [9]. The Raman spectra of $xLi_2O\cdot(1 - x)B_2O_3$ glasses consist of one component at 1030 cm^{-1} corresponding to B - O bond stretching of BO_4 units in diborate polycrystals and the others near 900, 940 and 1040 cm^{-1} correspond to the same vibration but in tetraborate units. Increasing concentration of Li_2O leads to the formation of pentaborate, tetraborate, diborate, metaborate and pyroborate [10]. The spectra of $Li_2O\cdot2B_2O_3$ fluxure show the features of crystalline nature with strong characteristic band at 783, 1034 and 1174 cm^{-1} and some weaker bands between 167 - 723 cm^{-1}. The spectra of the lithium metaborate ($Li_2O\cdot B_2O_3$) show the clear representation of 545 - 582, 765, 955, 1108 - 1128 and 1467 cm^{-1}. When the sample is heat treated above melting temperature, then the bands around 640, 671, 724 cm^{-1} and two less resolved bands in the range 1475 - 1495 cm^{-1} were also observed [100]. Raman spectra of $Li_2O\cdot4B_2O_3$ at room temperature indicate the formation of boroxol rings containing one BO_4 tetrahedron with increasing temperature, the stability of BO_3 tetrahedron decreases and finally, destroyed [101]. The networking structure of Li_2O-PbO-B_2O_3 is attributed by $[BO_{3/2}]^0$, $[B_2O_{4/2}]^-$ and B-O-B bending mode at 1485, 967 and 765 cm^{-1}, respectively. The band due to diborate units at 535 cm^{-1} is completely disappeared by the addition of PbO whereas a few additional bands in region 280 - 300 cm^{-1} are incorporated. The emergence of peaks in the region of 1200 cm^{-1} is associated with symmetric stretching of B_3 units and is generated during the incorporation of Pb - O into the structure. The band at 640 cm^{-1} region was attributed to a bending mode of the Pb - O - B links in the new structure [102]. The Raman spectra in range 150 - 1600 cm^{-1} of $(30 - x)Li_2O - xK_2O - 10CdO/ZnO - 59B_2O_3$ (x = 0, 10, 15, 20, and 30) doped with $1MnO_2/1Fe_2O_3$ showed the four region of bands as: (i) 190 - 600 cm^{-1}; (ii) 600 - 820 cm^{-1}; (iii) 900 - 1200 cm^{-1}; (iv) 1200 - 1600 cm^{-1}. The strong peaks around 775, 650, 500 cm^{-1} and a weak peak ~805 cm^{-1} are present, which are attributed to localized breathing motions of oxygen atoms in the boroxol ring. The peaks around 950 and 1110 cm^{-1} are occurred due to diborate groups in the structure. The peaks in the high frequency region are attributed to BO_2O^- triangles linked to BO_4 units and BO_2O triangles linked to other triangular units [103].

The polarized Raman spectra of sodium borate glasses showed the short range structure of BO_3 and BO_2O^- units. In HH (parallel to the inherent polarisation of the excitation laser) spectra, some strong Raman bands were found in frequency region 700 - 850 cm^{-1}. The strongest band due to boroxol ring was also observed at 805 cm^{-1} in the spectrum of glass. A broader and asymmetric band at lower frequency side was assigned with increase of Na_2O. A band near 1500 cm^{-1} was found in the spectra and it shifts toward lower frequency side with the increase of Na_2O concentration whereas VH (perpendicular to the inherent polarisation of the excitation laser) spectra showed drastic difference from HH spectra. VH spectra showed some more bands at 773, 730 and 670 cm^{-1} [104]. The spectra of B_2O_3-Na_2O glasses depict five major peaks at 480, 660, 770, 806 and 920 cm^{-1}. The peaks due to the isolated diborate groups and the ring-type metaborate groups polymerized by BO_3 and BO_4 units remain unaffected with addition of Al_2O_3 whereas peak at 770 cm^{-1} was shifted towards low frequency side in the spectrum. This means that BO_4 units were consumed and the boroxol ring $(B_3O_6)^{3-}$ gradually increased. Another new vibrational peak at about 920 cm^{-1} was appeared in 6 mol% Al_2O_3 content. This peak is the characteristic of orthoborate type structure containing BO_3 units, which can be transformed by the linking of pentaborate and tetraborate groups. The presence of orthoborate groups and absence of pentaborate groups proves the feasibility of the transformation pentaborate to the orthoborate groups with effect of Al_2O_3 effect on the structure. This suggests that the addition of Al_2O_3 destroyed the high polymeric borate units like pentaborate into the low polymeric groups such as boroxol rings, triborate and orthoborate groups [105]. There are four Raman bands in glassy matrix of $60B_2O_3\cdot$ $(20 - x)Na_2O\cdot10PbO\cdot10Al_2O_3{:}xTiO_2{:}yNd_2O_3$. The bands at 755 and 772 cm^{-1} were assigned due to chain type metaborate groups and the symmetric breathing vibration of six membered rings with one BO_4 tetrahedron, respectively. The position of boroxol ring was found at 797 cm^{-1} in this system. When TiO_2 concentration was increased, then back conversion of BO_4–BO_3 takes place. The incorporation of Ti^{4+} led to ~ 40% smooth reduction of the BO_4 groups due to the BO_4–BO_3 back conversion effect [12].

The Raman spectrum of lead borate glasses in glass compositions PbO 80%, Bi_2O_3 20% and PbO 90%, B_2O_3 10% showed a very sharp band at 130 cm^{-1} in first composition and shifted to 139 cm^{-1} in second composition. Few broad bands centred at 710, 905, 1024, 1239 and 1308 cm^{-1} are also observed in the pattern. In 1 mol% MoO_3 doped lead borate glass, two other peaks at 1927 and 3341 cm^{-1} are introduced. On increasing the doping concentration of MoO_3 the band near 1255 cm^{-1} become weaker. A sharp band at 133 cm^{-1} in the 2 mol% Mo-containing lead borate glasses was found. The Raman peak in un-doped lead borate glasses is assigned at 139 cm^{-1} and this band was located at 144 cm^{-1} in crystalline PbO. This suggests the presence of Pb^{2+} in high lead borate glasses in the form of PbO_4 groups. The sharp band observed at 305 cm^{-1} of lead borate glass containing 5 mol% of MoO_3 is not observed in un-doped lead borate glasses whereas it appeared at 296 cm^{-1} in crystalline lead oxide and 282 cm^{-1} in crystalline molybdenum trioxide MoO_3. This can be predicted as Raman band at 305 cm^{-1} is originated from different site of Pb^{2+}. The weak broad Raman band in MoO_3-lead borate glasses at 3311 - 3341 cm^{-1} are assigned due to molecular water [106]. Sodium-doped lead borate glasses in glass system $xNa_2O\cdot(100 - x)(10PbO\cdot 90B_2O_3)$, are made by structural units of boroxol ring resonance and growth of triborate [107]. The spectra of bismuth containing lead borate glasses showed Raman peaks at 400, 550, 710, 920 and 1220 cm^{-1}. The peaks for heavy metal oxides are assigned in the range 380 - 580 and 650 - 950 cm^{-1} due to the bridging anion modes and the non-bridging anion modes, respectively. The polarization behaviour of bismuth and lead cations have similar due to almost similar atomic weight. First two peaks correspond to the bridge-anion motion due to symmetric stretching of Bi - O - Bi and Pb - O - Pb combined with Bi - O - Pb [108]. The Raman spectra for the $xFe_2O_3\cdot(100 - x)[3B_2O_3\cdot 0.7PbO\cdot 0.3Ag_2O]$ glasses (Fig. 6) confirm the presence of boroxol rings [$B_3O_{4.5}$], pyro- $B_2O_5^{4-}$, ditri- [B_3O_8] and dipenta-borate [B_5O_{11}] groups as Raman bands are present at ~770, ~800, ~1040 and ~1340 cm^{-1}. A wide envelope appears around ~465 cm^{-1} due to isolated diborate groups as well as Pb - O linking vibrations and the envelope at ~700 cm^{-1} is the characteristic of symmetric breathing vibrations of metaborate rings. The silver ions shifted the peak at 806 to 800 cm^{-1}. With increasing Fe_2O_3 content in lead borate glasses containing silver decreases the intensity of peaks at 770 and 800 cm^{-1} and grow the band at 1040 and 1340 cm^{-1} [109]. The Raman bands in PbO - BaO - B_2O_3 glasses are assigned at 770, 806, 1230, 1280 and 1450 cm^{-1} [110]. The substitution of cadmium to lead in lead borate glasses was represented by Raman band in the range 200 - 300 cm^{-1}. The band near 840 cm^{-1} is not found and it suggests that CdO_4 is not formed in the glass network. Raman bands were found at 3691, 1275, 927, 720, 623 and 219 cm^{-1} in spectra of glass with composition $30PbO_2\cdot 20CdO\cdot 50B_2O_3$ [111].

Structure of barium borate glasses consist of mainly two band near 460 and 805 cm^{-1}. With the addition of 0.5 mol% Mn in glassy matrix, one more band about 990 cm^{-1} was assigned and the intensity of this band increases with increasing the concentration of Mn, i. e. MnO is helpful in formation of orthoborate group. The addition of Mn ions upto 3 mol% the band intensity of band ~ 460 cm^{-1} increases and thereafter decreases. There are two new bands at ~ 630 and 700 cm^{-1} are also introduced with the addition. The band at ~ 630 cm^{-1} was assigned due to vibration of ring and chain type of meta- and penta- borate groups whereas the band at 700 cm^{-1} is attributed to vibrations of chain or ring- type metaborate groups [112]. There

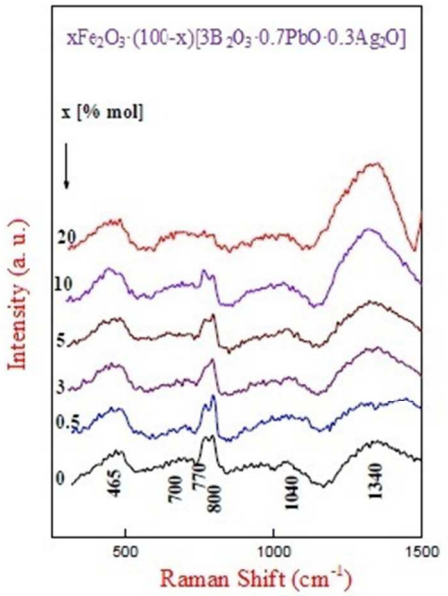

Fig. 6: Raman spectra for $xFe_2O_3\cdot(100 - x)[3B_2O_3\cdot 0.7PbO\cdot 0.3Ag_2O]$ glasses [109]

are five Raman bands at ~ 490, ~ 690, ~ 800, ~ 875 and ~ 1250 cm^{-1} that are present in $3B_2O_3$-As_2O_3 glass matrix. The band at ~ 490 cm^{-1} is caused by the vibrations of isolated diborate groups and/or to vibrations of As - O bonds. The band near 875 cm^{-1} decreases progressively with the addition of silver ions. The Raman spectra of $xAg_2O\cdot(1 - x)[zB_2O_3\cdot As_2O_3]$ (z = 1,2,3) glasses showed the bands at 490, 685, 803, 880, 960 and 1250 cm^{-1}. The addition of manganese ions in $xAg_2O\cdot(1 - x)[2B_2O_3\cdot As_2O_3]$ vitreous matrix leads to structural modifications and to increase of disorder degree, particularly for higher manganese ions concentrations ($y \geq 20$ %mol) in glass system $x[(1 - y)Ag_2O\cdot yMnO]\cdot(100 - x)[2B_2O_3\cdot As_2O_3]$ [113-114].

The Raman studies of $xSrO\cdot(1- x)B_2O_3$ ($0.2 \leq x \leq 0.7$) indicates the absence of band near 806 cm^{-1} band whereas presence of bands at 989, 677 and 552 cm^{-1} for x = 0.2. Raman spectra of $0.3SrO{:}0.7B_2O_3$ is dominated by the band at 671 cm^{-1} and assigned to di-pentaborate groups whereas for $0.4SrO\cdot 0.6B_2O_3$, a band at 799 cm^{-1} is observed. In glass sample with composition $0.5SrO\cdot 0.5B_2O_3$, the band near 744 cm^{-1} is attributed to six membered rings with one BO_4 tetrahedra. The intensity of this band decreases with addition of SrO. Addition of metal cations in these glasses introduced a new band near 423 cm^{-1}. The peak near 1413 cm^{-1} in undoped sample was shifted towards higher wavenumber side with addition on Fe^{2+}, Mn^{2+} and Zn^{2+} ions [115]. The structure of glasses in glass system $20MO.55Bi_2O_3.25B_2O_3$ (M = Sr, Ba) was determined by FT-Raman spectra. A broad Raman band at 124 cm^{-1} was observed in both barium bismuth borate and strontium bismuth borate glasses. A few resolved Raman bands are also present in region 50 - 400 cm^{-1}. These vibrations are assigned due to Bi atoms in the crystalline $Bi_{24}B_2O_{39}$. The external vibration due to α-Bi_2O_3 was appeared in the region 0 - 150 cm^{-1} while the internal vibrations

are ranges 150 - 500 cm^{-1}. The peak centred at ~128 cm^{-1} in the Raman spectra indicates the presence of $[BiO_3]$ and $[BiO_6]$ units in the structure of glass and glass ceramics. Raman bands at 696 and 723 cm^{-1} are associated with the symmetric bending vibration of $[BO_3]^{3-}$ anion in $Bi_{24}B_2O_{39}$ and indicate violation of the planarity of $[BO_3]^{3-}$ anion. The band due to boroxol ring at 804 cm^{-1} was disappeared during heat treatment of glasses. The bands at 773 cm^{-1} is predominant with associated bands at 960, 663 and 487 cm^{-1}. These bands are comparatively weak in barium bismuth borate glass ceramics as compared to strontium bismuth borate glass ceramics. The overtones of $[BO_3]^{3-}$ anion are observed in range 1100 - 1500 cm^{-1}. The strong band centred at ~1412 cm^{-1} was accredited to linked $[BO_3]^{3-}$ triangles with one free vertex as in BiB_3O_6 heat treated samples. The heat treatment of glasses increases the diborate units as indicated by the increased intensity of the bands 1117, 1031 and 930 cm^{-1} (strontium contained) and 1107, 1026 and 925 cm^{-1} (barium contained) [116]. The Raman study of Bi_2O_3-B_2O_3-ZnO-Li-O showed that Bi can form $[BiO_3]$ pyramidal or $[BiO_6]$ octahedral units. The symmetric stretching anion motion in an angularly constrained Bi - O - Bi configuration was found in region 300 - 600 cm^{-1}. The vibrations of Bi - O - Bi and $[BiO_6]$ octahedral units were present near 390 cm^{-1}. The position of this band is shifted towards lower wavenumber sides with increase of Li_2O. The shoulder around 555 cm^{-1} was assigned due to stretching vibrations of Bi - O- / Bi - O - Zn and its intensity increases with the increase of ZnO content. The Raman peak at 220 cm^{-1} indicates the presence of Zn - O tetrahedral bending vibrations of ZnO_4 units in the present glass system [14].

The polarized Raman spectra of zinc borate glasses showed features of binary metaborate glasses. The polarized bands were assigned at 950, 840 and 1280 cm^{-1}. The two weak bands at ~ 770 and 800 cm^{-1} were also observed Raman pattern. The unpolarized bands were found at 690 and 1420 cm^{-1}. The strongly polarized shoulder localized at about 250 cm^{-1} is ascribed to bending modes of ZnO_4 units. The doping of Eu^{3+} in zinc borate increases intensity of Raman band. The band at 440 cm^{-1} is assigned due to a Eu^{3+} - O stretching/ BO_3^{3-} vibrational mode [117]. The Raman spectra of glasses in glass system $60B_2O_3$-$10TeO_2$-$5TiO_2$-$24R_2O$:1CuO (where R = Li, Na, K) depict the bands of boroxol ring, vibrations of ring / chain type meta borate units and stretching vibrations of B - O^- bonds with non bridging oxygen. The networking modifying behaviour of Na_2O and K_2O is stronger than Li_2O [118].

Raman spectra of (1- x)$[3B_2O_3 \cdot K_2O] \cdot xTiO_2$ glasses consist of bands centred at 420, 475, 600, 670, 770, 800, 850, 930, 1230 and 1450 cm^{-1}. The intensity of band at 770 cm^{-1} is higher than that of band near 800 cm^{-1}. The band at 770 cm^{-1} is significant upto x = 0.2 and at higher concentration of titanium oxide, the intensity of bands at 420, 475 and 670 cm^{-1} were found to increase. For x = 0.5, two shoulders appear at 850 and 600 cm^{-1}. Further addition of TiO_2 introduces the appearance of ring type metaborate groups and loose BO_4^- tetrahedra. Therefore, the number of non-bridging oxygens increases with increasing titanium concentration and the glass structure becomes more randomized. The addition of K_2O in borate glasses changes the boron coordination number from 3 to 4 [119]. The calcium oxide modified the structure of borate glasses. The structure of borate glasses consist of boroxol groups, a smaller number of pentaborate groups, diborate groups, chain type metaborate groups and pyroborate groups at lower concentration of calcium oxide whereas at higher concentration of calcium oxide, pentaborate, orthoborate and metaborate groups are also appeared. With increasing the content of calcium oxide, the number of non-bridging oxygen ions increases [120]. The yttrium oxide in calcium borate glasses further modified structure [121]. The glasses with the compositions of $22.5Gd_2O_3 \cdot xWO_3 \cdot (47.5 - x)MoO_3 \cdot 30B_2O_3$ (x = 0 - 40) consisted by structural units centred at 344, 840 and 944 cm^{-1} as shown in Fig. 7. When these glasses were heat treated, then a few more sharp Raman bands were also introduced. The Raman peak at ~994 cm^{-1} was assigned due to symmetric stretching vibrations in $(WO_4)^{2-}$ tetrahedral unit in the glass composition with Sm_2O_3 for x = 10 [15]. Peak assignment of various vibrational units in borate glasses are listed in Table 1.

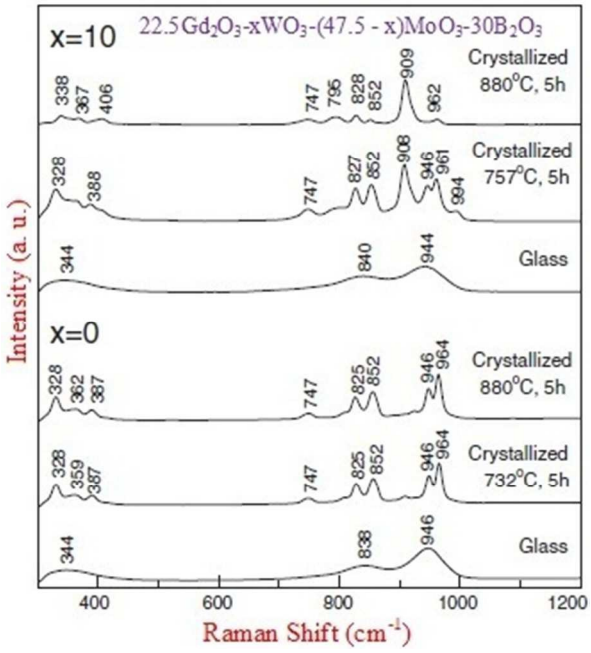

Fig. 7: Raman spectra of glasses in system $22.5Gd_2O_3 \cdot xWO_3 \cdot (47.5 - x)MoO_3 \cdot 30B_2O_3$ (x = 0 - 40) [15]. (Reproduced with permission of Elsevier)

Table 1: Assignment of main Raman bands in the spectra of borate glasses.

Wave number (cm^{-1})	Raman assignments	Reference
465 - 500	isolated diborate groups	105, 113-115
535	diborate units	102
600 – 650	symmetric breathing vibrations of metaborate rings	100, 103, 111, 115, 119
650-660	pentaborate groups	103, 105
700 - 735	symmetric breathing vibrations of metaborate chains	10, 100, 104, 12, 106, 108, 111, 116
740-775	Symmetric breathing vibrations of six membered rings with one BO_4^- tetrahedra units	10, 100, 104, 105, 12, 109, 115, 119
765	B-O-B bending mode	102
800-808	boroxol ring	99, 103, 105, 12,109, 112, 112-115, 117, 119
835-840	Pyroborate vibrations	115, 126

875 - 1000	ortho-borate groups	10, 105, 106, 108, 111, 112-114, 117, 119
1000-1110	diborate groups	10, 100, 102, 103, 106, 112-115
1200	symmetric stretching of B_3 units	102
1216 - 1260	Pyro-borate groups	102, 106, 108, 109, 119
1300 –1600	$B–O^-$ stretching in metaborate rings and chains	102, 106, 109, 115, 116
3300 - 3500	molecular water	102
0 - 150	external vibration of α-Bi_2O_3	116
128	presence of [BiO_3] and [BiO_6] units	116
150 - 500	internal vibrations of α-Bi_2O_3	116
220	Zn - O tetrahedral bending vibrations of ZnO_4 units	117
250	bending modes of ZnO_4 units	118
390	[BiO_6] octahedral units	117
300 - 600	angularly constrained Bi - O - Bi configuration	117
555	stretching vibrations of Bi - O- / Bi - O - Zn	117
440	Eu^{3+}-O stretching / BO_3^{3-} vibrational mode	118

3.2. Silicate Glasses

The networks of silicate glass are shown in Fig. 8. Raman spectroscopic studies of silicate glasses showed the formation of structural units of orthosilicate, silicon-oxygen stretching vibrations of tetrahedral silicate units, symmetric stretching vibrations of silicate tetrahedra, inter-tetrahedral Si - O - Si linkages and structural unit Q^n_{Si}, where Q represents the tetrahedral unit and n the number of bridging oxygen (BO) per tetrahedron. For silicon compounds, n varies between 0 and 4, where Si is a central tetrahedral atom ranging from Q^0 which represents orthosilicates SiO_4^{4-}, Q^4_{Si} (tectosilicates), Q^3_{Si}, Q^2_{Si} and Q^1_{Si} representing intermediate silicate structures.

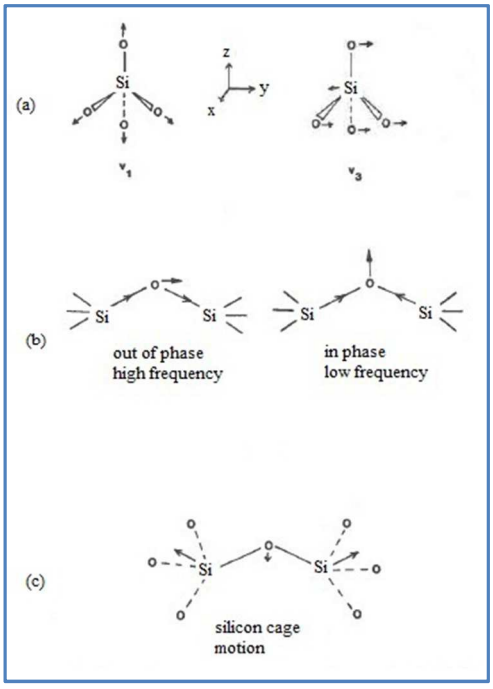

Fig. 8: The selected networks of silicate glasses [16]. (Reproduced with permission of Mineralogical Society of America)

These networks can be modified by adding certain network modifiers such as alkali and alkali earth atoms. The high frequency bands are described in mainly polarized Raman bands centred in the range 1050 - 1100, 950 - 1000, 900 and 850 cm^{-1}, they are designated as disilicate, metasilicate, pyrosilicate and orthosilicate, respectively. The low frequency bands are mainly associated with Si - O - Si linkage [16]. The presence of water group in SiO_2 glasses was confirmed by Raman band at 3598 cm^{-1}. The weak band near 2350 cm^{-1} was arisen due to Si - OH groups involved in intratetrahedral hydrogen bonding across an edge of the SiO_4 tetrahedron. The Si - OH stretching mode at 970 cm^{-1} is more prominent than other bands and showing that more silanol groups are present in comparison to suprasil. The bands at 430, 800, 1060 and 1200 cm^{-1} arises due to fundamental vibrations of the dry SiO_2 glass. The sharp peaks at 490 and 600 cm^{-1} are the characteristic of defect bands. Raman bands at 541 and 1100 cm^{-1} in the spectra of dry and wet sodium silicate glasses indicate the presence of SiO units (Q_{Si} , species: SiO_4 units with one nonbridging oxygen) and vibrations of the bridging oxygen in the Si - O - Si linkage, respectively. The shoulders peaks near 850, 960 and 1000 cm^{-1} suggest that the three components are present in the high-frequency envelope whereas four components near 970, 1060, 1100, and 1150 cm^{-1} are similar to hydrous sodium silicate glasses [17].

The effect of cations on symmetric vibrational wavenumber of NBO of Si - O - T in high frequency range is small, whereas the intensity of Raman peak increases with increasing the radius of cation. The scattering cross section increases in order of Li, Na, K, Rb and Cs [18]. The Raman spectrum of sulphur induced sodium calcium silicate glasses indicates the band due to sulphur ions is located at 990 cm^{-1}. Not only this band, but some other bands due to silicate network are also present in the pattern [19]. The presence of rare earth oxides in soda-lime-silicate glasses led to a shift of the peak positions at 1100, 790 and 550 cm^{-1} and attributed to Si - O - Si asymmetric stretching, Si - O - Si symmetric stretching and bending vibration, respectively. It was observed that peak position of bands at 1100 and 790 cm^{-1} are shifted towards low frequency side and peak at 550 cm^{-1} was shifted towards high frequency side with doping of lanthanide elements (La_2O_3, CeO_2, Nd_2O_3 and Gd_2O_3) into soda-lime-silicate glass. Y_2O_3 in soda-lime-silicate glass led the frequencies of peak position at 1100, 790 and 550 cm^{-1} shift towards high frequency side. The Q^n_{Si} species in soda-lime-silicate glasses changes as $Si_2O_7^{6-} + 2Si_2O_5^{2-} = 5SiO_3^{2-} + SiO_2$ with addition of lanthanide elements [20]. The band near 980 cm^{-1} was observed in both bulk (suprasil) and sol-gel silica glass. The defect mode bands at 493 and 606 cm^{-1} are also assigned in the matrix. Raman bands at ~356, ~264, ~207 and ~128 cm^{-1} in quartz crystal are attributed to lattice modes whereas the strong peak at ~465 cm^{-1} is the characteristic of symmetric stretching vibration. In the high-frequencies, the bands at ~807 and ~1083 cm^{-1} are assigned to Si - O - Si bending and SiO_4 asymmetric stretching vibration, respectively. The addition of CaO in silica glass changes the relative intensities of bands as indicated in Fig. 9. The intensity of band at 1050 cm^{-1} was increased due to addition of CaO. With addition of modifier content of MgO, peak position of 805 cm^{-1} is shifted towards lower wavenumber side. Comparatively, the CaO changes the structure more significantly than MgO [21-22].

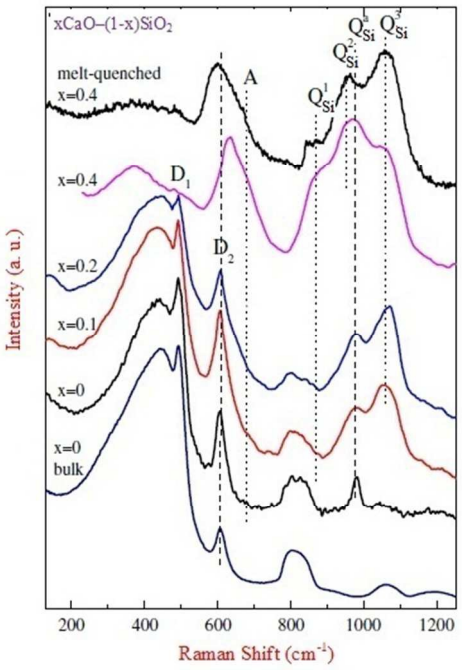

Fig. 9: Raman spectra of xCaO·(1 - x)SiO_2 (x = 0, 0·1, 0·2, 0·4) glasses [21]. (Reproduced with permission of Springer)

The main silicate structure is not much changed at smaller content of metal oxide, but two additional peaks are assigned at 500 and 600 cm^{-1}. The modifying nature of Cs, Rb, K, Na and Li in silica glass is in increasing order because the intensity of peak at 950 cm^{-1} increases in same order. The silicate bands are broaden in order Cs < Rb < K < Na < Li < Ca < Mg which may suggest that the perturbation of silicate units are increased with increasing cation strength [23].

Raman spectra of potash - lime - silica glasses depict the bands near 300 and 450 cm^{-1}. The addition of sulphur in glass matrix increases Raman cross-section of vibrational modes due to S - O bands in comparison to less polarized Si - O bonds. The intense Raman features in such glasses at 1000 - 1030 cm^{-1} indicates the mixture of three calcium sulphates: gypsum ($CaSO_4.2H_2O$), (1008 cm^{-1}), bassanite ($CaSO_4.1/2H_2O$) (1016 cm^{-1}) and anhydrite ($CaSO_4$), (1026 cm^{-1}). The bands in Raman spectra in the range of 608 - 679 cm^{-1} and 1110 - 1167 cm^{-1} are the feature of silicate networks whereas the peak in the range 412 - 494 cm^{-1} is the characteristic of cation–oxygen vibrational modes [24]. In Raman spectra of lead silicate glasses, a band near 1000 cm^{-1} was shifted towards longer wavelength side and becomes broader with increasing the content of lead. The intensity of Raman peak at 140 cm^{-1} was increased by increasing content of lead. Other peaks at 450, 950 and 1060 cm^{-1} are also modified by PbO. After UV irradiation with energy density 150 mJ/cm^2, the significant changes in the spectra were observed. The intensity of Pb - O band at 140 cm^{-1} was decreased after UV irradiation and no new band appears in the Raman spectra. The decrease of intensity after UV irradiation is caused by the broken Pb - O bond in lead silicate glasses and the broken Pb - O bond is related to the energy density of UV beam [25]. The lead silicate glasses provide a simple absorption spectrum gamma irradiation [122]. Band assignment of various vibrational units in silicate glasses are listed in Table 2.

Table 2: Assignment of main Raman bands in the spectra of silicate glasses.

Wave number (cm^{-1})	Raman assignments	Reference
580	Si–O^0 rocking motions in fully polymerized SiO_2 (Q^4) units	20
600	Si–O–Si bending vibration in depolymerized structural units	20
700–850	Si–O–Si symmetric stretching of bridging oxygen between tetrahedra	20
1050 - 1100	disilicate	16
950 - 1000	metasilicate	16
790	Si - O - Si symmetric stretching	20
807	Si - O - Si bending	21-22
850	Orthosilicate, SiO_4^{4-}	16
900	pyrosilicate	16
970	Si - OH stretching mode	17
1083	SiO_4 asymmetric stretching vibration	21-22
1100	Si - O - Si asymmetric stretching	20
2350	Si-OH groups involved in intratetrahedral hydrogen bonding across an edge of the SiO_4 tetrahedron	17

3.3. Phosphate Glasses

The typical Raman spectra of phosphate glass are shown in Fig. 10. The structure of the phosphate glasses are mainly consisted by Q_P^n groups of PO_4 tetrahedra (n = number of bridging oxygen per PO_4 tetrahedron). The symmetric stretching of P - O is assigned at 1260 cm^{-1} of an asymmetric profile (620 cm^{-1}), symmetric stretching vibration of P - O (1380 cm^{-1}), the symmetric stretching of a non bridging oxygen on a Q_P^2 tetrahedron at 1170 cm^{-1}, P - O - P symmetric vibrations at 690 cm^{-1}, the symmetric stretching of the orthophosphate groups PO_4^{3-} near 960 cm^{-1}. These bands are modified by dopants like earth and alkaline-earth atoms. Addition of TiO_2 upto 10 mol % reveals the depolymerization of the phosphate glass network by systematic conversion of Q_P^2 structural units into Q_P^1 and finally into Q_P^0 structural units. Even though Q_P^2 to Q_P^1 conversion is taking place due to breaking of P - O - P linkages, formation of P - O - Ti and P - O - Al linkages provide cross linking between short P-structural units. Above 10 mol % TiO_2 content, network is highly depolymerized due to the formation of Q_P^0 structural units and cross-linking becomes poor. The band near 700 cm^{-1} is assigned due to the symmetric stretching of P - O - P linkages in Q_P^2 and Q_P^1 structural unit. On addition of TiO_2 in phosphate glass, the intensity of the bands near 1280, 1170 and 700 cm^{-1} is decreased and a few new bands at 1210, 1090, 900, 750 and 625 cm^{-1} are introduced. The bands at 1210 and 1090 cm^{-1} are assigned due to asymmetric and symmetric stretching vibrations of PO_3 groups (Q^1 structural units), respectively. The coordination of Ti^{4+} ions by oxygen atoms is found in Raman spectra and band near 625 cm^{-1} is attributed to the vibration of octahedral titanate units TiO_6, as its relative intensity increases with increasing TiO_2. The band centred at 930 cm^{-1} is associated with shorter Ti - O bond than for octrahedral titanium and attributed to the titanyl bonds (Ti - O or -Ti - O - Ti-) associated with a five coordinated Ti. The band at 900 and 525 cm^{-1} are related with asymmetric stretching of P - O - P bridges and bending vibrations of P - O bonds, respectively [123]. The

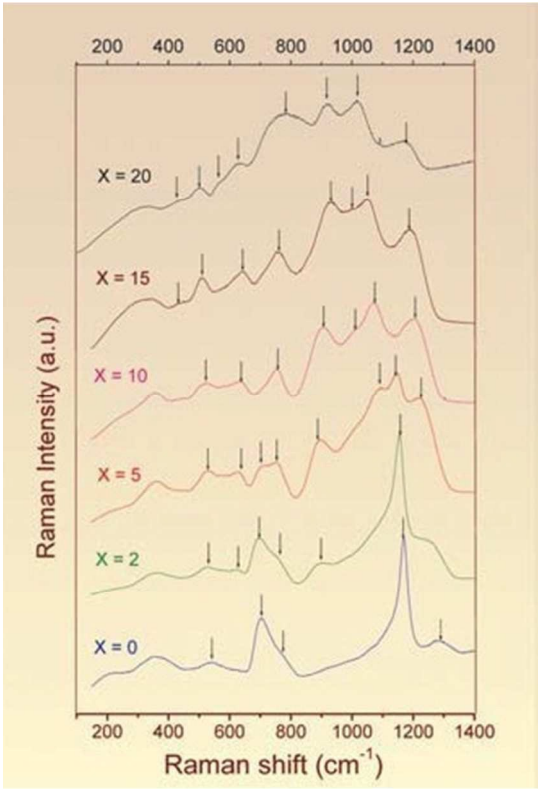

Fig. 10: Raman spectra of $40Na_2O$-$10Al_2O_3$-$xTiO_2$-$(50-x)P_2O_5$ glasses [123]

bands in Raman spectra of $39AlF_3 \cdot 11NaF \cdot 10LiF \cdot (40-x)CaF_2 \cdot MgF_2 \cdot SrF_2 \cdot BaF_2 \cdot xNaPO_3$ system at 515, 570, and 620 cm^{-1} is assigned to octahedral $[ALF_6]$, five-coordinated $[AlF_5]$ and tetrahedral $[AlF_4]$ structural units, respectively. The intensity of band at 1330 cm^{-1} decreases whereas, the intensity of bands at 1070, 860 and 775 cm^{-1} increases with increase of phosphate content. The low frequency band at 70 cm^{-1} is boson band. Raman peaks at 250 and near range 350 - 420 cm^{-1} are associated with symmetric stretching vibrations of fluorine species bonded by the modifying cations [124]. The bands at 1194, 1294 and 1349 cm^{-1} are prominent in Raman spectra of Na_2O-Al_2O_3-P_2O_5. With increasing the content of Al_2O_3, intensity of bands near 1200 cm^{-1} is enhanced whereas the band at 1161 cm^{-1} is disappeared. The band at 676 cm^{-1} is shifted towards higher wavenumber side due to formation of aluminium metaphosphate structure. Due to introduction of Al_2O_3, the band located at 1349 cm^{-1} is disappeared. The weak vibration due to PO_2 bending and in chains of O - P - O bending motions is assigned at 300 and 360 cm^{-1}, respectively. With addition of Fe_2O_3 in this glass system, the intensity of the bands at 1257, 1185 and 706 cm^{-1} is increased whereas position of band of at 1349 cm^{-1} is shifted to 1309 cm^{-1} due to depolymerization. The ferric oxide in sodium phosphate glasses forms the structure of metaphosphate and connected by P - O - Fe bonds [125]. The bands in Raman spectrum of zinc-alumino-sodium-phosphate glasses with addition of Pr^{3+} and Nd^{3+} are located at 545, 698, 1042 and 1162 cm^{-1} [126]. Raman spectra of $55P_2O_5 \cdot 30CaO \cdot (25 - x)Na_2O \cdot xTiO_2$ ($0 \le x \le 5$) system have bands near 695, 705, 930, 1180, 1280 and 1370 cm^{-1}. The band at 930 cm^{-1} is attributed to Ti-O band and the intensity of band at 1370 cm^{-1} is increased by addition of TiO_2 upto 5 mol% [127]. Raman spectra of Li_2O-BaO-Al_2O_3-La_2O_3-P_2O_5 glasses showed the bands are found at 1850, 1700, 1180 and 700 cm^{-1} [128]. The spectra of phosphate glasses containing TiO_2 consist of bands which are assigned at 340 - 540, 693 - 697, 1010 - 1020, 1160 - 1173, 1248 - 1271 cm^{-1}. The band in range 1010 - 1020 cm^{-1} is disappeared at higher content of TiO_2 and peak at 905 cm^{-1} is assigned to asymmetric TiO_5 [129].

Raman investigations of $xMoO_3.(100 - x)[P_2O_5.CaO]$, $0 \le x \le 50$ mol% glass system showed that Raman bands are centred at 316, 392, 536, 693, 1175 and 1274 cm^{-1}. The addition of MoO_3 about $0.3 \le x \le 1$ mol%, a new band at 1032 cm^{-1} is introduced. The intensity of band at 683 cm^{-1} was decreased at $5 \le x \le 10$ mol% of MoO_3 whereas peak at 436 is shifted towards higher wavenumber side. The band located at 700 cm^{-1} becomes weaker and the peak at 1270 cm^{-1} is disappeared. MoO_3 is strong modifier and forms the vibration at 600 cm^{-1} due to asymmetric vibration of (Mo - O - Mo). The band at 894 cm^{-1} is caused to orthomolybdate, $(MoO_4)^{2-}$ units. The band at 963 cm^{-1} is assigned due to stretching vibrations of partially isolated Mo - O bonds in deformed (MoO_6) units [130]. The structure of $xCaO \cdot (100 - x)(0.4Fe_2O_3 \cdot 0.6P_2O_5)$ (x = 0, 10, 20, 30, 40, 50 mol%) glasses are made by structural units of phosphate and modified by calcium as well as iron. Their Raman bands are observed at 626, 772, 950, 1071 and 1241 cm^{-1} [131]. Raman spectra of calcium coacervate show the peaks, which are found at 1168 and 698 cm^{-1}. The Raman spectrum of the croconate ion consist of bands located at 564, 649, 1605 and 1722 cm^{-1} [132]. In Raman spectra of glasses of glass system $xGa_2O_3 \cdot (1 - x)P_2O_5$, there are five Raman bands are observed at 1320, 1210, 715, 620 and 350 cm^{-1}. The depolarization by Na, Ca, Zn, Mg, Al and Be is found at 350 cm^{-1}. The low frequency band is assigned due to Ga - O - M bridges. The band near 640 cm^{-1} is assigned in gallate system with four fold coordinated Ga atoms [133-134].

The structure of PbO-MoO_3-P_2O_5 glasses is formed by networks of phosphate units and modified by MoO_3. The incorporation of MoO_3 results the transformation of octahedral MoO_6 units into tetrahedral MoO_4 units. The band at 930 cm^{-1} is shifted towards high frequency side with increasing content of MoO_3. The intense band near 1158 cm^{-1} is shifted towards lower frequency side with increasing content of MoO_3. The bands in region 850 - 970 cm^{-1} are attributed to Mo - O and Mo - O bonds in MoO_6 tetrahedra [135]. The structure of PbO–Ga_2O_3–P_2O_5 glasses doped with Cr_2O_3 is modified by forming tetrahedral CrO_4^{2-} structural units. The phosphate network is modified by all Pb, Ga and Cr ions. The band at 398 cm^{-1} is assigned due to Ga - O - P linkages and peak at 368 cm^{-1} is attributed to GaO_6 vibrational groups. The band at 270 cm^{-1} is associated with Cr-O vibrations of CrO_4^{2-} units [136]. Lead phosphate network can also be modified by Zn and Cu ions. The phosphate network after modification is assigned at positions 690, 747, 904, 1026 and 1155 cm^{-1}. The intensity of band 1155 cm^{-1} is decreased with addition of BaO [137]. High ZnO content in lead phosphate glasses forms the network of P - O - Zn bonds [138]. The network of lead–gallium phosphate glasses can be modified by rare earth ions (Eu^{3+}, Dy^{3+}, Tb^{3+}, Er^{3+}). The spectrum contains two shoulders centred at 1050 and 1120 cm^{-1} corresponds to symmetric stretching vibration of diphosphates in Q^1 units. The other two shoulders near 900 and 1250 cm^{-1} are attributed to symmetric stretching vibration of the PO_4 in the Q_P^0 units and asymmetric stretching vibration of the PO_2 in Q_P^2 units, respectively. The high frequency band about 1120 cm^{-1} is related to phonon energy of the lead phosphate glass and its intensity decreases, when the PbO is substituted by the PbF_2 components

[139]. The bands near 1172, 1096, 1032, 973, 930, 742, 627 and 474 cm^{-1} are found in the glasses in the system $PbO\text{-}Fe_2O_3\text{-}P_2O_5$. The bands at 1080 and 966 cm^{-1} are related to $[P_2O_7]^{2-}$ and terminal $[PO_3]^{2-}$ symmetric groups in Q_P^1 pyrophosphates [140]. In_2O_3 in $PbO\text{-}P_2O_5\text{-}As_2O_3$ plays an important role in network modification and form the structural unit of InO_6. The band centred at 200 cm^{-1} is related with In - O vibrations of InO_6 structural units. The band near 110 and 250 - 350 cm^{-1} is attributed to Pb - O ionic bond vibrations and PbO_4 structural vibrations, respectively. With increasing the concentration of In_2O_3, the intensity of the bands due to symmetric vibrations of the phosphate groups is increased whereas, the intensity of bands due to torsional vibrations of PO_4 structural units and As_2O_3 structural vibrations is decreased [141]. The fraction of orthophosphate Q_P^0 units in lead iron phosphate glasses increases with increasing Cr_2O_3 content. The band at 600 cm^{-1} is assigned due to the different P - O, Fe - O and Pb - O stretching and bending modes. The intense peak is assigned at 1062 cm^{-1} in Cr free glass. The intensity of band at 979 cm^{-1} is enhanced with Cr addition. The ferric oxide also forms the network of Fe - O stretching vibration in FeO_6 octahedra in $\alpha\text{-}Fe_2O_3$ and it is indicated by band near 614 cm^{-1} [142-143].

The Raman spectra of iron phosphate glasses investigated by Milankovic et.al showed that network of phosphate glasses are modified by incorporation of MoO_3. Addition of MoO_3 in glass matrix replaced the stronger P - O - P bonds with a weaker Mo - O - P bonds as the bond covalence decreases from P - O to Mo - O and the bands located at 850 and 980 cm^{-1} become stronger. The iron works as network modifier for phosphate network and band assigned at 400 cm^{-1} due to PO_4 polyhedra was modified by it. The Raman band near 864 cm^{-1} is associated with the stretching mode of isolated orthomolybdate $(MoO_4)^{2-}$. Due to increase of NBO and increase of $(PO_4)^{3-}$, some bands show the splitting in the spectra. The asymmetric vibration of Mo-O-Mo is assigned at 620 cm^{-1}, whereas symmetric Mo - O - Mo vibrational mode is appeared at 520 cm^{-1} [144]. The addition of La_2O_3 in iron phosphate glasses lowers the peak position of band at 1072 cm^{-1} and increases the relative area of band at 1231 cm^{-1} whereas decreases for band at 1072 cm^{-1}. This results is related with depolymerization of phosphate network $2\,Q_P^1 = Q_P^2 + Q_P^0$ [145]. The most intense peak in Raman spectra of cesium doped iron phosphate glasses is assigned at 1085 cm^{-1} due to Q_P^1. This band is shifted towards lower wavenumber side with increase of Cs content. The intensity of band at 555 cm^{-1} is enhanced due to disproportion of pyrophosphate linkage. The intensity of this band increases with increase of cesium loading and indicates the increasing concentration of orthophosphate units. The bands at 270 and 200 cm^{-1} are related with bending vibrations of P - O - P and Cs - O vibrations, respectively [146]. The P - O - P network is depolymerized with increasing CeO_2 content in glass compositions and results the conversion of Q_P^1 to Q_P^2 structural units. The addition of CeO_2 in iron phosphate glasses introduced some new bands near 1000, 1150 and 1279 cm^{-1}. The band at 1037 cm^{-1} is shifted towards higher wavenumber side with the substitution of FeO_3 by CeO_2. The band at 522 cm^{-1} is related to Fe - O bonds and a new peak at 460 cm^{-1} is attributed to cerium oxygen polyhedron vibration of $[CeO_8]$ unit symmetrical stretching mode at higher content of CO_2 [147]. The depolymerization of the phosphate network, in the form of conversion of Q_P^1 to Q_P^0 groups ($2\,Q_P^n + Na_2O = 2\,Q_P^{n-1}$), is take place with the addition of Na_2SO_4 content and results the conversion of P - O - P bridging oxygens to P - O - Na^+ non-bridging oxygens. The band at 1039 cm^{-1} is shifted to higher frequency region with addition of modifier Na_2O ($Na_2SO_4 = Na_2O + SO_3$) content. The intensity of the band at 931 cm^{-1} is also increased with this addition [148]. The vibrations at 170, 306 and 420 cm^{-1} arise due to network vibrations and librations of Fe - O polyhedral and phosphate network units, respectively. The peak position of 1090 cm^{-1} is shifted towards low wavenumber side with heat treatment at transition temperature of glass [149].

The MoO_3 plays an important role for modification in structural units of glass system $ZnF_2\text{-}Bi_2O_3\text{-}P_2O_5$. With addition of MoO_3 in glass matrix form the structural units of MoO_4 and MoO_6. The intensity of band due to asymmetric vibrations of Mo - O - Mo linkages with increase in dopant concentration is observed to increase with a slight shift in the position towards lower wavenumber. In Raman spectra of motioned system, bands due to BiO_6 and BiO_3 pyramidal structural units are assigned at 547 and 230 cm^{-1}, respectively. The modifier Zn takes the interstitial positions in the form of dangling bonds along with non-bridging oxygens as Zn - O - P linkages and fluorine breaks the P - O network [150-151]. The doping of WO_3 in place of MoO_3 forms the network of bending vibrations of O - W - O with corner shared octahedra. The noticeable decrease in the intensity of W - O stretching was also observed which is associated WO_4 tetrahedral units as given in Fig. 11 [152]. Trivalent samarium doped K - Mg - Al zinc fluorophosphate glasses are formed by networks of phosphate and modifiers by K, Mg, Al, Zn and F. The stretching vibration of Al - O linkages in AlO_4 structural units was observed [153-154]. The structure of $2P_2O_5$ - CaO - 0.05ZnO glass matrix contains Raman bands near 345, 460, 903, 959, 1011, 1137, 1168, 1297 and 1400 cm^{-1}. The content of Ag_2O in the glass system modified the network of ring structures. The slight depolymerization was also taken place in glass matrix. Raman spectra of $xAg_2O\cdot(100 - x)[2P_2O_5\cdot CaO\cdot 0.05ZnO]$ confirm the modifying nature of Ca, Zn and Ag. With increasing content of Ag_2O, the intensity of band near 554 cm^{-1} is increased and the peak position of band at 690 cm^{-1} is shifted towards lower frequency side due to change in the chain P - O - P bond angles. The silver oxide favours the presence of orthophosphate, pyrophosphate and small metaphosphate chains, these informations are revealed by the increase in intensity of the bands at 554, 1100 and 670 cm^{-1} [155].

Raman spectroscopic investigations of $TiO_2\text{-}P_2O_5\text{-}CaO$ glasses showed that the structure consists of a distorted Ti octahedral linked to pyrophosphate unit through P - O - Ti bonds at higher content of TiO_2 and thus, the depolymerization was take place in P - O - P network. In Raman spectra of TiO_2 free calcium phosphate glasses, the strong bands near 680, 1175 and 1290 cm^{-1} are assigned in the glassy network whereas with addition of TiO_2, the existed bands are disappeared. The new bands at 765 and 920 cm^{-1} are also introduced with TiO_2 addition [156]. Li_2O further modified the network of $TiO_2\text{-}P_2O_5\text{-}CaO$ glasses [157]. Raman spectra of ($P_2O_5\text{-}K_2O\text{-}Al_2O_3\text{-}CaF_2$) glasses depict the bands at 335, 543, 625, 728, 1075, 1135 and 1284 cm^{-1}. The band centred at 728 cm^{-1} is related with vibrations of P - F chain formation,

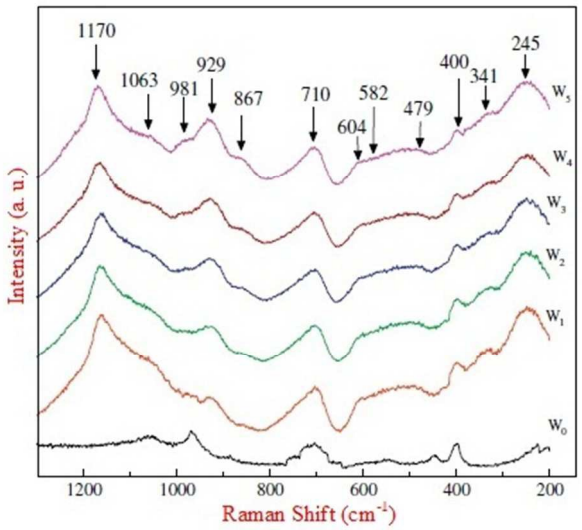

Fig. 11: Raman spectra of $ZnF_2{\cdot}Bi_2O_3{\cdot}P_2O_5$ glass-ceramics doped with different concentrations of WO_3 [152]. (Reproduced with permission of Elsevier)

whereas less intense band at 625 cm^{-1} is assigned due to Al_2O vibrations. The band at 335 cm^{-1} is attributed to K_2O [158-159]. CuO and V_2O_5 work as network modifier for calcium phosphate glasses. At higher concentration of CuO and V_2O_5, the glass matrix forms the network of V - O - P and Cu - O - P. The band assigned at 1175 cm^{-1} indicates the depolymerization of phosphate network. The band at 980 cm^{-1} is related with V - O vibration in VO_5 tetragonal pyramid and stretching vibrations of O - V - O in metavanadate chains are assigned at 970-905 cm^{-1} [160]. Raman spectra of $(50 - y)Na_2O.yCuO.10Bi_2O_3.40P_2O_5$ ($0 \leq y \leq 25$ mol%) glasses depict the formation of P - O - Bi and P - O - Cu bonds. Bi_2O_3 acts as network modifier and is incorporated in the form of BiO_6 units. No depolymerization was taken place with the replacement of Na_2O by CuO [161]. As CuO content increases in $xCuO{\cdot}(1 - x)P_2O_5$ glasses, the intensity of the P - O band associated with the Q^3 Cu tetrahedra increases to $x < 0.33$ and decreases with a concomitant increase of the intensity of the band at 1265 cm^{-1} due to the asymmetric vibration of the PO_2 groups on Q^2 tetrahedra. When $x > 0.33$, the isolated Cu-octahedra begin to share common oxygens to form a sub-network in the phosphate matrix. The intensity of band at 640 cm^{-1} increases with addition of CuO. CuO in phosphate glasses promotes the depolymerization effects [162].

Raman spectra of cadmium phosphate glasses reveal the formation of P - O - V and V - O - V bonds instead of P - O - P vibrations after addition of V_2O_5. The presence of band at 760 cm^{-1} is attributed to V - O - V vibration. The intensity of bands at 615 and 974 cm^{-1} is increased with addition of V_2O_5 about 20 mol%. These bands are related with P - O - V and V - O vibration VO_5 trigonal bipyramids, respectively [163]. The Li^+ and Cd^{2+} cations in the phosphate glass network are responsible for shifting the bands as well as intensity modification. The band at 1120 cm^{-1} is shifted towards high frequency side with increase of Li_2O content [164]. With increasing the content of BaO in lithium barium phosphate glasses, the intensity of all bands is enhanced. The bands at 712 and 1163 cm^{-1} are shifted slightly towards low wavenumber side with increase of BaO. The decrease in wavenumber is related with an increase of average length of the P - O bond resulting from π-bond delocalization on the Q_P^3 tetrahedra [165]. Raman spectra of phosphate glasses with addition of Er^{3+} / Yb^{3+} ions depict 312, 380, 685, 1165 and 1275 cm^{-1} [166]. The assignment of main Raman bands in the spectra of phosphate glasses are listed in Table 3.

Table 3: Assignment of main Raman bands in the spectra of phosphate glasses.

Wave number (cm^{-1})	Raman assignments	Reference
1300-1350	P=O stretching of terminal oxygen	123
1267-1294	PO_2 asymmetric stretching of non-bridging oxygen , in Q^2 units	123
1260, 1380	symmetric stretching of P - O	123
1210	asymmetric stretching vibrations of PO_3 groups	123
1170	symmetric stretching of a non bridging oxygen on a Q_P^2 tetrahedron	123
1161	PO_2 symmetric stretching of non-bridging oxygen , in Q^2 units	123
1065-1097	PO_2 symmetric stretching of non-bridging oxygen , in Q^1 units	123
1090	symmetric stretching vibrations of PO_3 groups	123
1080	$[P_2O_7]^{2-}$ symmetric groups in Q_P^1 pyrophosphates	140
966	terminal $[PO_3]^{2-}$ symmetric groups in Q_P^1 pyrophosphates	140
960	symmetric stretching of the orthophosphate groups PO_4^{3-}	123
940	PO_2 symmetric stretching of non-bridging oxygen , in Q^0 units	123
900	asymmetric stretching of P - O - P bridges	123
700	the symmetric stretching of P - O - P linkages in Q_P^2 and Q_P^1 structural unit	123
690	P - O - P symmetric vibrations	123
676-708	P-O-P symmetric stretching of bridging oxygen, in Q^2 units	123
525	bending vibrations of P - O bonds	123
390-410	O-P-O bending modes	123
398	Ga - O - P linkages	136
360	chains of O - P - O bending motions	125
300	PO_2 bending O - P - O bending motions	125

3.4. Borosilicate Glasses

Typical Raman spectra of alkali borosilicate glasses are shown in Fig. 12. The network structure of borosilicate glasses is formed by borate as well as silicate structural units. The structure of lithium silicate glasses consists of Raman bands at 850 cm^{-1} (Q_{Si}^2), 950 cm^{-1} (Q_{Si}^2), 1000 cm^{-1} (Q_{Si}^3), 1050 cm^{-1} (Q_{Si}^3), 1080 cm^{-1} (Q_{Si}^3) and 1150 cm^{-1} (Q_{Si}^4). The borosilicate structure is associated with the vibrational modes of the two medium-range (400 to 850 cm^{-1}) order superstructures, reedmergnerite $[BSi_3O_8]^-$ and danburite $[B_2Si_2O_8]^{2-}$ and high frequency region (850 - 1250 cm^{-1}) vibration related with silicon Q_{Si}^n vibrational modes [167]. Raman spectra of sodium borosilicate glasses depict the bands centred at 350, 500, 630, 670, 770 and 808 cm^{-1}. The bands between 300 and 500 cm^{-1} are attributed to mixed stretching and

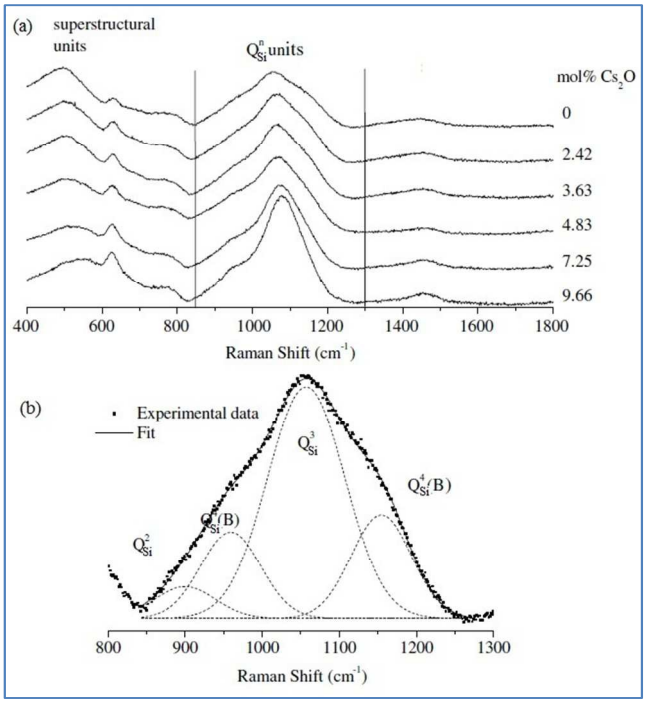

Fig. 12: Raman spectra of alkali borosilicate glasses [167]. (Reproduced with permission of Elsevier)

bending modes of Si-O-Si units. The bands in the range 550 - 850 cm^{-1} are caused by ring breathing modes. The bands at 670, 770 and 808 cm^{-1} are the signature of tetraborate groups, four- and three-coordinated boron in diborate and boroxol rings, respectively. The intensity of peak at 808 cm^{-1} decreases with increase of sodium content whereas the band near 770 cm^{-1} shows opposite behaviour. This means sodium ions favour the formation of BO_4^- units at the expense of BO_3 units. The polymerization of the silicate network first increases with Na_2O content upto Na_2O/B_2O_3 = 0.6 and thereafter decreases with the increase of Na_2O content [168]. Sulphate in borosilicate glass showed its presence in the form of vibrational modes of SO_4 tetrhedra. The major bands of sulphate, assigned at 1100, 1000, 990, 620 and 460 cm^{-1} are related to asymmetric S - O stretch modes, symmetric S - O stretching, symmetric S - O stretch vibrations of tetrahedral SO_4^{2-}, asymmetric O - S - O bend modes and symmetric O - S - O bend modes, respectively [169]. When the B_2O_3 content is increased, the broad bands near 1500 and 800 cm^{-1} are developed. The shoulder peak at 590 cm^{-1} is assigned due to symmetric oxygen breathing vibrations of three-membered siloxane rings. The network modifier ions Na^+ and Ba^{2+} are used for conversion of BO_3 units into BO_4 units before forming non bridging oxygen (NBO) in the network. As the silica content increases in the glassy matrix and the ratio Na/Si (or Ba/Si) decreases, which could depolymerise the silicate network after forming BO_4 units increases. It can be concluded that the silicate network in SiO_2-rich borosilicate glasses remains more polymerized than in boron-rich glasses [170]. The bands in the range 1200 - 1100 cm^{-1} are disappeared as the ratio B_2O_3/Na_2O becomes zero. The intensity of the band at 1077 cm^{-1} is also increased. With increasing amount of Na_2O in the glass, the intensity of band around 630 cm^{-1} was increased and the band in the range 550 - 450 cm^{-1} begins to dominate, which results from formation of $[BO_4]$ tetrahedral of small degree of polymerization. The intensities of bands at 385, 360, 287, 1850 and 1975 cm^{-1} are increased with increasing ratio $B_2O_3/(Na_2O + 3La_2F_6)$ [171]. When barium is substituted for the sodium cation, the position of the peak at 540 cm^{-1} is shifted to low frequency region and the intensity of band at 635 cm^{-1} was decreased. The high frequency band around 1100 cm^{-1} becomes strongest with sodium introduction. The substitution of Ba and Ca cations enhances the intensity of 960 cm^{-1} and shifted towards the low frequency [172]. The Raman spectra of Na_2O-B_2O_3-SiO_2 exhibit the bands at ~430, 485, 600, 800, 1060 and 1200 cm^{-1}. The bands around 485 and 600 cm^{-1} (known as defect lines D_1 and D_2) are assigned due to the ring breathing mode of four and three-membered silicate rings, respectively. Raman peaks at 770 and 805 cm^{-1} become more significant for glasses with higher borate content [173]. In Raman spectra of $30Na_2O{\cdot}5SiO_2{\cdot}65[(1 - x)P_2O_5{\cdot}xB_2O_3]$ glasses, the intensity of bands at 680 and 770 cm^{-1} decreases with increase of B_2O_3, which are attributed to the $(P - O - P)_{sym}$ stretching vibration and BO_4 stretching in borate species, respectively. The bands at 1200 and 1350 cm^{-1} are disappeared for x = 0.250. The intensity at 620 cm^{-1} increases with an increase in B_2O_3 content. The bands at 500, 780 and 1100 cm^{-1} are appeared in B_2O_3 rich glasses. The Raman band at 1160 cm^{-1} is attributed to the symmetric stretching mode of the terminal oxygen on each tetrahedron. The intensity of band at 780 cm^{-1} increases and assigned to BO_3 stretching vibration [174]. The intensity of Raman bands at 810 cm^{-1} is increased whereas decreased for band at 795 cm^{-1} by heat treatment of glasses [175]. The S-O symmetrical stretching modes near 1000 cm^{-1} from tetrahedral SO_4 environments was observed. The peak near 300 cm^{-1} is assigned to S - S stretch in the dithionate anion $S_2O_6^{2-}$ [176-177].

The wettability of the diamond by the borosilicate glass melt at temperatures above 700 °C was enhanced due to the oxidation of the diamonds. The irregular pores become distinct in the diamond–borosilicate glass composites sintered above 800 °C [178]. The depolarization of silicate network takes place with increase of zirconia and causes to reduction of intensity of band due to Si - O - Si links. Some of the highly polymerized Q^3_{Si} and Q^4_{Si} units are replaced by the less polymerized Q^2_{Si} units in the glass structure. The most borate units within the glass structure are probably linked to silicate tetrahedral in range 650 - 800 cm^{-1} and it is indicated by the lack of any prominent peaks in this range. The band near 703 cm^{-1} is related to the zirconia network (Zr - O stretch) [179]. The structure of Eu^{3+} ions doped MgO-PbO-B_2O_3-SiO_2-Nd_2O_3 glasses consist of bands centred at 1510, 1385, 955, 842, 732, 645, 487 and 298 cm^{-1} (Fig. 13). The last band near 298 cm^{-1} was attributed to Ln - O - Ln (Nd, Eu) stretching vibrations. The position of first band was shifted towards higher wavenumber side with increase of doping concentration of Eu. The bands at 605 and 527 cm^{-1} are related to B - O - Si linkages along with PbO_4 units and Si - O - Pb, respectively. The polymerization of the glass network take place due to the replacement of bonds B - O - B, Si - O - Si with more resistant B - O - Si, Si - O - Pb bonds with addition of Eu^{3+} ions [180]. The structural units of TiO_4 exist in CaO-B_2O_3-SiO_2-TiO_2 glasses and the degree of depolarization decreases with increase of CaO/SiO_2 ratio. The increase in B_2O_3 leads to increase of BO_4

tetrahedral units in glass matrix. The addition of TiO_2 in this glass system introduces two peaks near 840 and 726 cm^{-1} whereas the existed bands at 500 - 800 cm^{-1} are disappeared. The bands near 948, 1040 and 1300 - 1500 cm^{-1} are shifted towards low frequency side. The bands at 840 and 726 cm^{-1} are the characteristic of Ti - O - Si or Ti - O - Ti vibrations and deformation of O - Ti - O or O - (Si, Ti) - O in chain or sheet units or both [181].

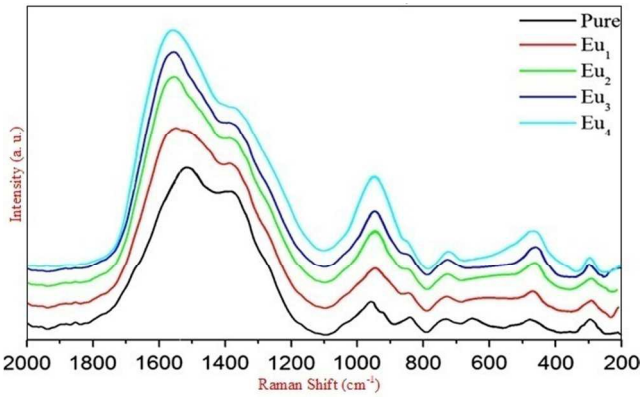

Fig. 13: Raman spectra of MgO-PbO-B_2O_3-SiO_2-Nd_2O_3-Eu_2O_3 glasses [180]. (Reproduced with permission of Elsevier)

The structure of borosilicate glass in presence of modifier BaO also contains the network of borate and silicate. The addition of BaO decreases the intensity of band near 816 cm^{-1}. A new band at 780 cm^{-1} is incorporated at 42 mol % of BaO. The bands at ~843, 877, 934, 1000 and 1040 cm^{-1} are shifted to the lower frequency region and cause to low network polymerization after formation of BO_4 units due to the increment of BaO content instead of SiO_2 [182]. The position of peak at 675 cm^{-1} is shifted towards higher wavenumber side with increasing ratio of BaO/SrO. This is associated with variation of ionic radii of Ba and Sr. La_2O_3 and Fe_2O_3 in barium strontium titanate (BST) borosilicate glasses changes the peak positions of 675 and 820 cm^{-1} towards higher wavenumber side [183-185]. Raman band about 735 cm^{-1} occurs due to metaborate groups and symmetric breathing vibrations of BO_3 triangles replaced by boron tetrahedral (BO_4). Raman shift has been shifted towards high wavenumber side with increasing the doping concentration of Fe_2O_3 [52]. Raman spectra of AO-SiO_2-B_2O_3-La_2O_3, (A = Mg, Ca, Sr, Ba) glasses showed bands near 770 - 779 and 1274 - 1280 cm^{-1}, which are related to borate network. The bands near 796 - 800 and 1060 - 1070 cm^{-1} caused to silicate network. Tetrahedral coordination occurs in both silicon and boron in this glass system. Lanthanum is occupied interstitial octahedral co-ordination in the local network. The modifiers, such as Ba, Ca, Mg, Sr and La, break the B - O or Si - O bonds and occupy interstitial or substitutional position in glass network. As the ionic radii of modifier ion increase in order $Mg^{2+} > Ca^{2+} > Sr^{2+} > Ba^{2+}$, then polarization follow the Fajan's rule, i.e. weak polarization by Mg and strong polarization by Ba [186]. Raman spectra of lead bismuth borosilicate glasses show the bands at 1582 and 1382 cm^{-1} in high frequency region [187]. After irradiation, the peak at 480 cm^{-1} is shifted toward higher wave number side. This suggests that the decrease of the Si - O - Si bond angle is decreased. A new weak peak at 605 cm^{-1} is introduced by irradiation in glasses and assigned due to the D_2 defect peak involving the three-membered rings of SiO_4 tetrahedra. The weak band at 630 cm^{-1} is associated either with the hindered bending vibration of ring-type metaborate groups or the breathing mode of danburite-like rings. The Q^n_{Si} species of silicon remain almost unchanged after Ar-irradiatation [188]. The Raman band assignments of borosilicate glasses are listed in Table 4.

Table 4: Assignment of main Raman bands in the spectra of borosilicate glasses

Wave number (cm^{-1})	Raman assignments	Reference
1510-1570	B–O stretching modes involving with one NBO of [BO_3] triangles and molecular oxygen stretching vibration modes	183-185
1385-1397	Stretching vibrations of B–O^- bond in BO_4 units from different borate groups	183-185
1160	symmetric stretching mode of the terminal oxygen on each tetrahedron	174
947-955	Stretching vibrations of Si–O bond and due some presence of BO_4 units	183-185
840-842	Pyroborate unit along with ortho-silicate $(SiO_4)^{4-}$ composition or vibrations of Ti-O-Si or Ti-O-Ti structural units	181
808	boroxol rings	168
722-732	Chain-type metaborate groups containing NBO or deformation of O-Ti-O or O-(Si, Ti)-O in chain or sheet units or both	181
550-850	Ring breathing modes	167, 168
400 – 850	reedmergnerite $[BSi_3O_8]^-$ and danburite $[B_2Si_2O_8]^{2-}$	167
605	B – O – Si linkages along with PbO_4 units	180
590	symmetric oxygen breathing vibrations of three-membered siloxane rings	170
300-500	Mixed stretching and bending modes of Si-O-Si units	167
475-487	Si–O–Si, Si–O–B isolated vibrations	180

3.5. Borophosphate Glasses

Typical Raman spectra tin borophosphate glasses are shown in Fig. 14. In this study, it was found that the Raman bands centred at 1330, 1270, 1050, 1000, 950, 760, 700 cm^{-1} and some bands near 500 cm^{-1}. The vibrations at 1330 and 700 cm^{-1} are attributed to metaborate groups whereas the band near 1000 cm^{-1} is attributed to pyrophosphate or orthophosphate units. The presence of metaborate chains in glass matrix was found by the vibration at 760 cm^{-1}. The evidence of pyrophosphate units was also confirmed by peak located at 1050 cm^{-1}. The vibration at 1270 cm^{-1} is caused by orthoborate/pyroborate units [189]. Network of lithium borophosphate glasses, in presence of germanium oxide, consists of stretching vibrations of phosphate structural units in high (1000 - 1300 cm^{-1}) and mid frequency regions (500 - 700 cm^{-1}) and these units are modified by Ge ions. Ge free glasses showed a band at 1159 cm^{-1}, which is caused by metaphosphate structure. The vibration at 1260 cm^{-1} is related with asymmetric, $\nu_{as}(PO_2)$, stretching mode in Q^2_P units whereas the weaker band centred at 1093 cm^{-1} is attributed to $\nu_s(PO_3)$, in Q^1_P units. The bands at 703 and 665 cm^{-1} are assigned due to the symmetric stretching mode of P - O - P bridging bond in Q^1_P and Q^2_P structure, respectively. A broad band around 320 cm^{-1} is attributed to the cage vibrational frequencies of Li^+ ions. The addition of 5 mol.% GeO_2 shifted the band around 1159 to 1106

cm^{-1} and also showed depolymerization of the Q_P^2 structure by the formation of more Q_P^1 phosphate units. The intensity of band at 665 cm^{-1} is reduced with increasing GeO_2 and it is completely

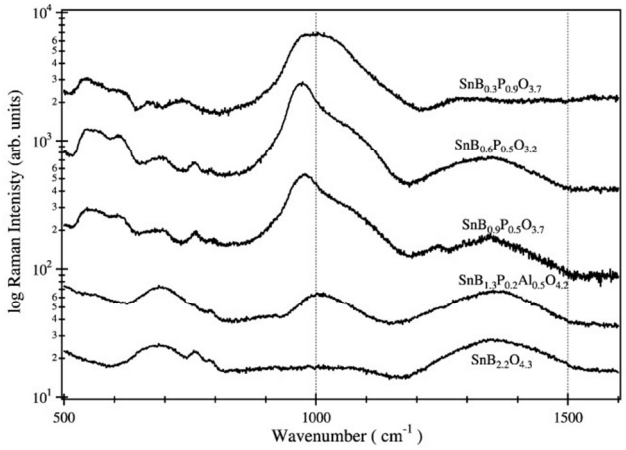

Fig. 14: Raman spectra of various tin borophosphate glasses [189]. (Reproduced with permission of Elsevier)

disappeared for 15 to 25 mol% of GeO_2 whereas the intensity of bands at 700 and 751 cm^{-1} are enhanced due to more depolymerization of Q_P^1 units by this addition. A new band at 600 cm^{-1} is introduced due to Ge - O - Ge bending modes or Ge - O - P stretching modes [190]. The four intense bands at 650, 696, 880 and 1112 cm^{-1} are found in Raman spectrum of $75P_2O_5$-$20B_2O_3$-$4.9Na_2O$-$0.1Er_2O_3$ glass [191].

The Raman bands at 636 and 350 cm^{-1} in Na_2O-Ga_2O_3-P_2O_5 glasses are attributed to GaO_4 and GaO_6 groups, respectively. The band centred at 515 and 540 cm^{-1} are caused by Ga - O - Ga bonds between GaO_4 tetrahedra and the band at 675 cm^{-1} is associated with the vibrations involved with non-bridging oxygens from the GaO_4 tetrahedra. The band at ~540 cm^{-1} was attributed to $[GaO_4]^-$. In Ti containing glasses, a intense band near 900 cm^{-1} is caused by $[TiO_4]$ groups [192]. Raman spectra of calcium borophosphate consisted by networks of ortho Q_P^0 and pyro Q_P^1 phosphate units. With addition of 20 mol% of B_2O_3 in calcium phosphate glass, the band 1045 cm^{-1} is shifted to 1038 cm^{-1} and new bands at 1000 and 675 cm^{-1} are also introduced [193]. In Raman spectra of $(1 - x)[0.5K_2O{\cdot}0.1B_2O_3{\cdot}0.4P_2O_5]{\cdot}xNb_2O_5$ glasses, a strong band in region 907 - 911 cm^{-1} was observed and the band of phosphate groups are assigned at 1070 - 1148 cm^{-1} and 1212 - 1244 cm^{-1}. The new bands at 811 - 817 and 638 cm^{-1} are introduced in glasses for more than 16.7 mol% Nb_2O_5. The vibrations centred at 907 cm^{-1} are the characteristic of symmetric stretching vibration of isolated NbO_6 octahedra. The dominating bands at 817 and 638 - 648 cm^{-1} are assigned due to Nb - O - Nb bonds in glass with 37.5 mol% of Nb_2O_5. The bands at 820 - 840 cm^{-1} in barium-potassium niobato-phosphate glasses are attributed to the deformation vibrational modes of Nb - O - Nb bridges between NbO_6 octahedra [194].

Raman spectroscopic studies of $50PbO{\cdot}10B_2O_3{\cdot}40P_2O_5{\cdot}xTiO_2$ glasses showed that major bands are located at 329, 729, 936, 1100 and 1210 cm^{-1} (Fig. 15). The strong peak at 1100 and 1210 cm^{-1} are shifted towards lower wavenumber side whereas the peak at 729 and 936 cm^{-1} are shifted towards higher wavenumber side with increasing the content of TiO_2 [195]. TeO_2 in lead borophosphate glasses form the structural units of TeO_3 and TeO_4 at its low and high concentrations, respectively. The intensity of band at 1092 cm^{-1} decreases with TeO_2 and also shifted towards low frequency side. This change is associated with depolymerisation of the phosphate network. The bands at 550 and 850 cm^{-1} are attributed to the vibration of oxygen atoms in P - O - P bridges and are gradually replaced by the band characteristic of different Te - O vibrations. New bands in the region 453 - 458 cm^{-1} are ascribed due to bending vibrations of O - Te - O and Te - O - Te linkages. The bands lying at 620 - 630 cm^{-1}, 660 - 670 cm^{-1} are related to stretching vibrations of TeO_4 trigonal bipyramids, whereas, the vibrations at 720 - 750 cm^{-1} and 760 - 800 cm^{-1} are associated with stretching vibrations of TeO_3 trigonal pyramids [196].

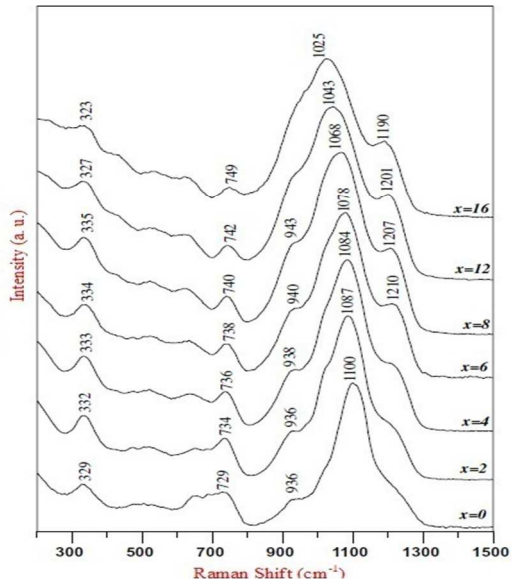

Fig. 15: Raman spectra of the glass series $50PbO$-$10B_2O_3$-$40P_2O_5$ +$xTiO_2$ [196]. (Reproduced with permission of Elsevier)

Zinc oxide plays an important role in modification of borate and phosphate structural units. In the spectra, a sharp band assigned at 808 cm^{-1} is the characteristic of B_2O_3 and the band at 968 cm^{-1} is caused by vibrations of isolated PO_4 units in the structural network of borophosphate glasses [197]. If TiO_2 was added in zinc borophosphate glasses, then, the intense bands at 1162 and 666 cm^{-1} are shifted towards to lower frequency side whereas, the band at 747 cm^{-1} is shifted to 774 cm^{-1} successively. The band at 506 cm^{-1} was disappeared above 4 mol% of TiO_2. The shifts of bands are associated with distortion of borate and phosphate units. The shift in sodium contained glasses is lesser as compared to Zn modified glasses due to difference in ionic field strength [198]. All the Raman bands are shifted towards lower wavenumber side with substitution of Sb_2O_3 instead of TiO_2 in above glass system. The vibrations of structural units containing Sb - O are assigned in the range of 350 - 700 cm^{-1}. Sb_2O_3 modifies the network in the form of SbO_3 units with single atom of Sb. The low concentration of Sb_2O_3 forms the isolated SbO_3 unit. The existence of three bands in place of two is associated with the splitting of the symmetry of SbO_3 units in the glass network. Sb_2O_3 content replicate the depolymerisation of phosphate chains. Raman bands in the range of 520 - 690 cm^{-1} are

attributed to SbO_3 pyramids. SbO_3 units linked into chains and clusters with Sb - O - Sb bridges at higher Sb_2O_3 content and are confined by bands in the region 380 - 520 cm^{-1} [199]. MoO_3 weakened the bond strength for zinc borophosphate glasses. The presence of the polarized vibrational band at 976 cm^{-1} is associated with MO_x symmetric stretching vibrations and the depolarized band at 878 cm^{-1} is ascribed due to the Mo - O - Mo stretching vibration. The incorporation of molybdate units in glass matrix is responsible for depolymerization of phosphate chains and the formation of P - O - Mo bonds [200]. The tellurium oxide in above glass system forms structural units of TeO_3, TeO_{3+1} and TeO_4. The phosphate units are depolymerized by incorporation of TeO_2 and also boron coordination is modified. When the ratio of B_2O_3/P_2O_5 increases, then TeO_4 units are replaced by TeO_3 units as the number of oxygen atoms in the glass is decreased [201-204]. The peak assignment of Raman spectra of borophosphate glasses are listed in Table 5.

Table 5: Assignment of Raman bands in the spectra of borophosphate glasses.

Wave number (cm^{-1})	Raman assignments	Reference
1260, 1380	symmetric stretching of P - O	123
1210	asymmetric stretching vibrations of PO_3 groups	123
1170	symmetric stretching of a non bridging oxygen on a Q_P^2 tetrahedron	123
1080	$[P_2O_7]^{2-}$ symmetric groups in Q_P^1 pyrophosphates	140
966	terminal $[PO_3]^{2-}$ symmetric groups in Q_P^1 pyrophosphates	140
960	symmetric stretching of the orthophosphate groups PO_4^{3-}	123
600	Ge - O - Ge bending modes or Ge - O - P stretching modes	190
550, 850	vibration of oxygen atoms in P - O - P bridges	196
968	vibrations of isolated PO_4 units	199

3.6 Aluminosilicate Glasses

Raman spectra of glasses for glass system $5Na_2O{\cdot}20CaO{\cdot}5Al_2O_3{\cdot}(60 - x)SiO_2{\cdot}xZnO$ (where x = 0, 4, 7 and 10 mol%) showed the bands by deconvolution, which are centred at 868, 956, 1020 and 1075 cm^{-1} and attributed to the Si\NBO stretching modes of mainly silicate units, Q_{Si}^n (Fig. 16]. The band near 868 cm^{-1} is the characteristic of Q_{Si}^1. The peak at 956 cm^{-1} is assigned due to Q_{Si}^2 whereas peak at 1019 cm^{-1} is the cause of asymmetric stretching of BO and related to Q_{Si}^1 - Q_{Si}^3 units. The band at 1020 cm^{-1} is associated with Q_{Si}^3. Raman bands in wavenumber range 400 - 800 cm^{-1} are assigned at 412, 544, 622 and 779 cm^{-1}. The vibrations in the range 400 - 650 cm^{-1} are caused by bending vibrations of the bridging oxygen (BO) bonds of SiO_4 and band near 779 cm^{-1} is caused by the Si - O - Si network, ZnO_4 tetrahedra and AlO_4 units with three BOs and one NBO. The low frequency bands located at 222, 279 and 338 cm^{-1} are related with cations of modifying networks. The vibration of cations Na^+ and Ca^{2+} are centred at 222 and 279 cm^{-1}, respectively. The coupled vibration of Ca - O and SiO_4 network are found at 338 cm^{-1}. The addition of ZnO in glass matrix shifts

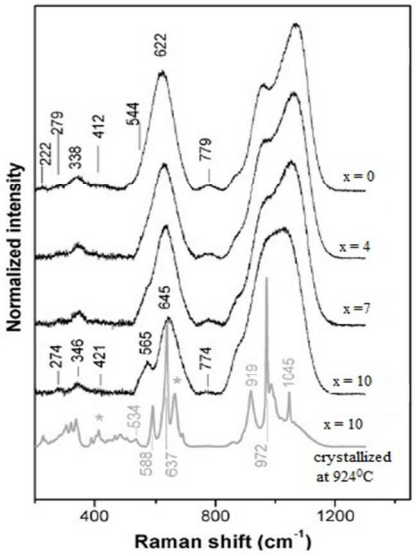

Fig. 16: Raman spectra of glasses for glass system $5Na_2O{\cdot}20CaO{\cdot}5Al_2O_3{\cdot}(60 - x)SiO_2{\cdot}xZnO$ [203]. (Reproduced with permission of Elsevier)

the bands at 279 and 338 cm^{-1} to position 274 and 346 cm^{-1}, respectively. With increasing ZnO/SiO_2 molar ratio, the band at 622 cm^{-1} is shifted towards 645 cm^{-1} and finally, splited into two components for 10 mol% ZnO content glasses [203].

Sodium silicate and aluminosilicate can be analyzed by Raman spectroscopy in low frequency region of 20 - 250 cm^{-1}. In this region, the peak at 69 cm^{-1} is the signature of Raman scattering involving in rotational motions of interconnected tetrahedral units. The position of this peak is shifted to 78 cm^{-1} with addition of Al_2O_3 upto 6 mol%. Raman peak at 170 cm^{-1} is assigned due to narrower distribution of T - O - T angles, or by a structural localization of those vibrations in specific clusters of molecules in the glass network. The band centred at 490 cm^{-1} is shifted to 482 cm^{-1}. The band at 597 cm^{-1} becomes broader with increase of content of Al/(Al + Na). This result suggests the presence of three-membered rings in the glass network. Raman band located at 781 cm^{-1} is shifted to 799 cm^{-1} with replacement of Na_2O by Al_2O_3. A shoulder near 810 - 820 cm^{-1} is the feature of Si - O stretching involving oxygen motions in the Si - O - Si plane or to the motion of the Si atom in its oxygen cage or threefold - degenerate rigid cage vibrational mode of TO_2 units. The high frequency bands at 960, 1070, 1100, 1150 and 1200 cm^{-1} are the characteristic of silicate network and vibrational modes of TO_4 tetrahedra [204]. A Raman band at 495 cm^{-1} was observed in albite glass and showed the presence of polymeric structure in such glasses. The band assigned at 595 cm^{-1} is the characteristic of structural defect in the glass involving T - O (non-bridging) vibrations (Fig. 17). The defect line, D_2, of SiO_2 is assigned at 606 cm^{-1}. The Al in borosilicate glass shifted the band positioned at 950 cm^{-1} to 900 cm^{-1} while peaks at 980 and 1110 cm^{-1} showed opposite trend with previous result. The polymerization become more significant with increasing Al/Na ratio [205].

The structure of aluminosilicate glasses consists of silicate and aluminate networks. The band centred at 1060 and 1200 cm^{-1} are attributed to Si - O stretching vibrations of SiO_4 tetrahedra. The intensities of bands at 1000 and 1100 cm^{-1} are increased with increase of Al_2O_3. This increase in the intensity of these bands is

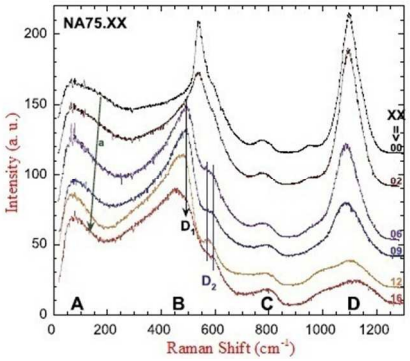

Fig. 17: Raman spectra of $75SiO_2·(25 - x)Na_2O·xAl_2O_3$ glasses [204]. (Reproduced with permission of Elsevier)

due to interlinking of Si-O-Al network. The intensity of band at 435 cm^{-1} was decreased with increase of Al_2O_3 and suggested to decrease of Si - O - Si linkage in tetrahedral units [206]. Aluminosilicate glasses along with silica-calcium, silica sodium aluminate and silica-potassium aluminate showed the appearance of bands centred at 1120, 1100, 930 and 890 cm^{-1}. The degree of metal cations induced network clustering increases in order of K < Na < Li < Ca < Mg within the SiO_2-$MAlO_2$ glasses (M = K, Na, Li, Ca and Mg) [207-208]. The low frequency bands at 450, 500 and 600 cm^{-1} are associated with motions of bridged oxygen in T - O - T linkages and band at 560 cm^{-1} in Al rich sample is caused by presence of Al - O - Al bridges in CaO-Al_2O_3-SiO_2 system. The intensity of band at 800 cm^{-1} was decreased with decrease of SiO_2 and shifted towards lower wavenumber side. The high frequency Raman spectra consist of peaks at 1000 and 1080 cm^{-1}. Al coordination exists mainly in four-fold type and varies between Q^2_{Si} and Q^4_{Si} species as a function of MO/Al_2O_3 ratio (M = Ca, Sr, Ba). At very higher concentration of CaO (more than 62 mol %) a Raman band between 300 - 400 cm^{-1} was also present. A Raman band at 170 cm^{-1} and a shoulder around 300 cm^{-1} was observed in Ba contend glasses. The intensity of peak at 170 cm^{-1} increases with Ba content. The peak position of Raman bands due to metal cation decreases with size of cation [209-212]. Raman band located at 450 cm^{-1} is the characteristic of motion of bridging oxygen in the plane perpendicular to the Si - O - Si (A1) bond. The vibration at 710 cm^{-1} gives the evidence of AlO_4 tetrahedra and the band at 760 cm^{-1} corresponds to the stretching mode of the Al - O bond with aluminium in four-fold coordination. The band at 960 cm^{-1} in the spectra is caused by stretching vibration of silicon-oxygen tetrhedra with two corners shared with aluminium-oxygen or calcium-oxygen polyhedral [213]. The depolarization ratio in calcium alumino-silicate glasses is 0.007 and 0.485 for intense bands at 540 and 96 cm^{-1}, respectively. This result showed that the vibration at 540 cm^{-1} is highly symmetric in nature. The polarized spectra for this glass system showed peaks centred at 96, 540, 767 and 867 cm^{-1}. Similar bands are also observed in other glass system with a slight variation in their peak positions [214]. The main peak assignment in the Raman spectra of Aluminosilicate glasses are listed in Table 6.

Table 6: Assignment of Raman bands in the spectra of Aluminosilicate glasses

Wave number (cm^{-1})	Raman assignments	Reference
1060, 1200	Si - O stretching vibrations of SiO_4 tetrahedra	206
960	stretching vibration of silicon-oxygen tetrhedra with two corners shared with aluminium-oxygen or calcium-oxygen polyhedral	213
810 - 820	Si - O stretching involving oxygen motions in the Si - O - Si plane or to the motion of the Si atom in its oxygen cage or threefold - degenerate rigid cage vibrational mode of TO_2 units	204
779	Si - O - Si network, ZnO_4 tetrahedra and AlO_4 units with three BOs and one NBO	203
450, 500, 600	motions of bridged oxygen in T - O - T linkages	209-212
400 - 650	bending vibrations of the bridging oxygen (BO) bonds of SiO	203

3.7 Phosphosilicate Glasses

A typical Raman spectrum of phosphosilicate glass is shown in Fig. 18 [215]. Raman spectra of phosphosilicate glasses consist of networks of phosphate as well as silicate. Raman peak at 1320 cm^{-1} is attributed to stretching vibrations of O - P double bonds and the bands below 860 cm^{-1} are assigned due to Si - O and P - O bonds in Si - O - Si, P - O - Si and P - O - P linkages. The peaks at 1200 and 1020 cm^{-1} are caused by P - O - P linkages and band near 1145 cm^{-1} is due to P - O - Si linkages [215-216]. The bands are located at 340, 426, 580, 648, 720, 780, 882, 956, 1040 and 1450 cm^{-1} in the Raman spectra of various compositions of CaO-MgO-SiO_2 system doped with B_2O_3, P_2O_5, Na_2O and CaF_2 (Fig. 19).

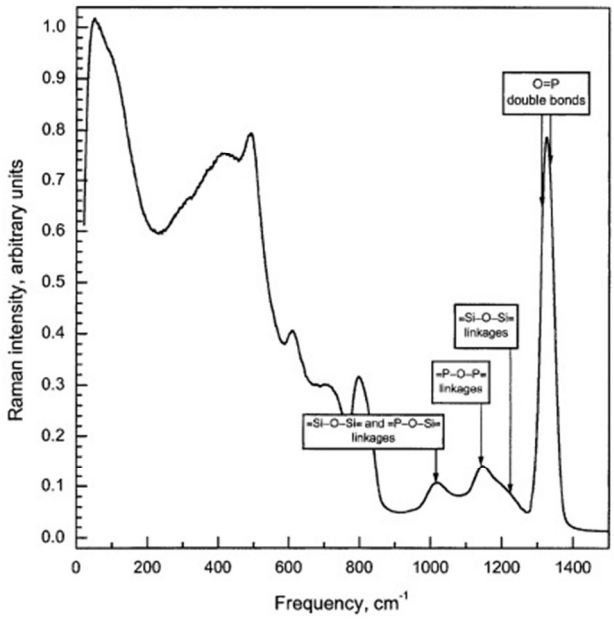

Fig. 18: Raman spectrum of phosphosilicate glass [215]. (Reproduced with permission of Elsevier)

The vibrations in the regions 800 -1300 cm^{-1} are the characteristic of the asymmetric vibration of SiO_4 tetrahedra whereas the bands

at 952, 590 and 425 cm^{-1} are assigned due to the symmetric

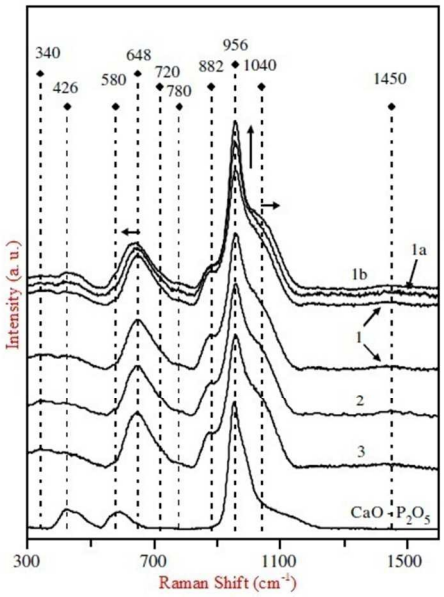

Fig. 19: Raman spectra of calcium magnesium silicate glasses doped with B_2O_3, P_2O_5, Na_2O and CaF_2 [217]. (Reproduced with permission of Elsevier)

stretching of the P - O^- bonds and O - P - O bending modes of the orthophosphate PO_4^{3-} unit (Q_P^2), respectively [217]. The silicate networks Si - O - Si and intensity of the Si - O - NBO stretching mode are modified by cations Na, Mg and Ca [218-219]. The addition of silver in calcium phosphosilicate glasses changes some networks such as the contribution of Q_P^0, Q_P^3 and Q_P^4 is progressively vanishing by increasing the concentration of silver and a weak band around 1025 cm^{-1} was also assigned. The position of band at 956 cm^{-1} was shifted at 967 cm^{-1} with this addition. The spectra also show the occurrence of a depolymerization process of SiO_4 network [220]. The average distance between silicates, phosphates, inter silicate-phosphate and aluminium–phosphate chains was increased by increasing the concentrations of AlO_6 structural units and it leads to the increase in the average bond length of Tm - O and Er - O due to weaker field around Tm - O and Er - O ions [221]. The main peak assignment in the Raman spectra of Phosphosilicate glasses are listed in Table 7.

Table 7: Assignment of Raman bands in the spectra of Phosphosilicate glasses

Wave number (cm^{-1})	Raman assignments	Reference
1320	stretching vibrations of O - P double bon	215-216
1200, 1020	P - O - P linkages	215-216
1145	P - O - Si linkages	215-216
860	Si - O and P - O bonds in Si - O - Si, P - O - Si and P - O - P linkages	215-216

3.8 Alumino-borosilicate Glasses

Raman spectra of NaF alumino-borosilicate glass consist of vibrations located at 1075, 947, 802, 723 and 480 cm^{-1} (Fig. 20). The Raman band located at 802 cm^{-1} is the characteristic of Si - O - Si vibration and symmetric breathing vibration of the boroxol rings. Sodium fluoride (NaF) in alumino-borosilicate glass increases the stability of boroxol ring. The metaborate group is assigned at 723 cm^{-1} whereas lower intensity bands centered at 1075, 947 and 480 cm^{-1} are attributed to the stretching vibration of Si - O - Si and B - O - Si. Instead of above bands, few more bands at 1114, 1000, 885, 770, 657, 598, 520, 491 and 447 cm^{-1} are also assigned in Raman spectrum. The band located at 1114 cm^{-1} is attributed to diborate groups. The band at 885 cm^{-1} indicates the presence of pyroborate groups. The existence of symmetric breathing vibration of six-membered rings BO_4 tetrahedron was confirmed by band located at 770 cm^{-1}. The bands at 1000 and 520 cm^{-1} indicate the availability of the vibration of Si - O^-. B - O - B, B - O - Si and Si - O - Si bending. The rocking vibration is also found in network of glass at 475 cm^{-1}. Raman band at 951 cm^{-1} is attributed to B - O - Si stretching vibration. The shoulder peak at 447 cm^{-1} is assigned due to the bending or rocking vibrations of the B - O - Si linkages, B - O - B, B - O - Si and Si - O - Si [222].

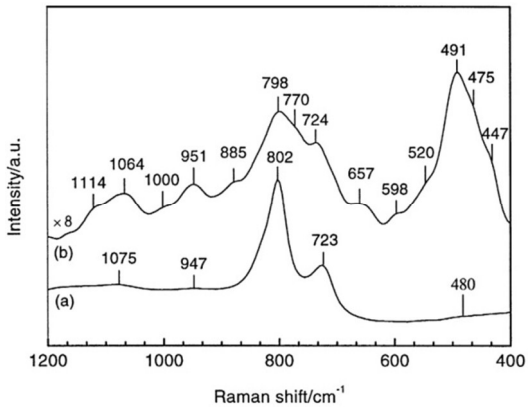

Fig. 20: Raman spectra of NaF alumino-borosilicate glasses [222]. (Reproduced with permission of Elsevier)

Raman spectroscopy of sodium-alumino-borosilicate glasses in presence of Gd_2O_3 showed that the band at 1050 cm^{-1} is shifted towards lower wavenumbers side with addition of Gd_2O_3 and intensity of band centred at 450 cm^{-1} was increased. One more band at 300 cm^{-1} was ascribed for the glasses with 7.06 and 13.58 mol% of Gd_2O_3. The borate network was much influence by network modifying cations as compared to silicate network. Gd cations are more effective than Na cations for modifications of network [223]. Raman spectra of strontium alumino-borosilicate glasses exhibit vibrations of borate as well as silicate network along with some linking networks. The asymmetric ring breathing vibrations is assigned at 430 cm^{-1}, symmetric stretching vibrations of Si - O - Si at 800 cm^{-1}, stretching vibrations associated to SiO_4 composed of sites with three and four-fold rings ranging 1000 - 1200 cm^{-1} and symmetric stretching vibrations at 1200 cm^{-1}. The borate networks are pure B_2O_3 exhibit a strong band at 805 cm^{-1} due to symmetric beating vibrations of boroxol ring oxygen. The boroxol ring structure is splited into different ring structures (i.e. triborate, tetraborate or pentaborate, etc.) in the presence of suitable modifiers in the glass network (Fig. 21). After the irradiation of γ-ray, the intensity of bands due to asymmetric vibrations was increased and shifted to higher wavenumber side. The effect of radiation was lesser in Al_2O_3 added glasses [224]. Not only γ-ray irradiation but also β-

ray changes the network of the glasses. The bending vibration of Si - O - Si at 460 cm^{-1} is shifted in the glasses irradiated with 10^9 Gy. β-ray radiation was decreases the Q^2_{Si} species as compared to Q^3_{Si} ones [225-226]. The β-ray irradiation in rare earth alumino-borosilicate glasses reduces the Cr and Mn ions from the matrix. The Raman band at 460 cm^{-1} is shifted to 480 cm^{-1} with adding the Cr instead of Sm and Gd. Silicate networks in the range 900-1200 cm^{-1} are not much affected by Cr whereas new bands centered at 845 and 900 cm^{-1} are introduced in the matrix. The behaviour of Raman band at ~ 1550 cm^{-1} due to molecular oxygen could not be analyzed under irradiation due to polishing of glass surface [226-229]. Similar to β-ray irradiation, the γ-irradiation is effective for reducing Sm^{3+} to Sm^{2+} ions from 10 kGy dose [230]. The Raman band assignment in Alumino-borosilicate glasses are listed in Table 8.

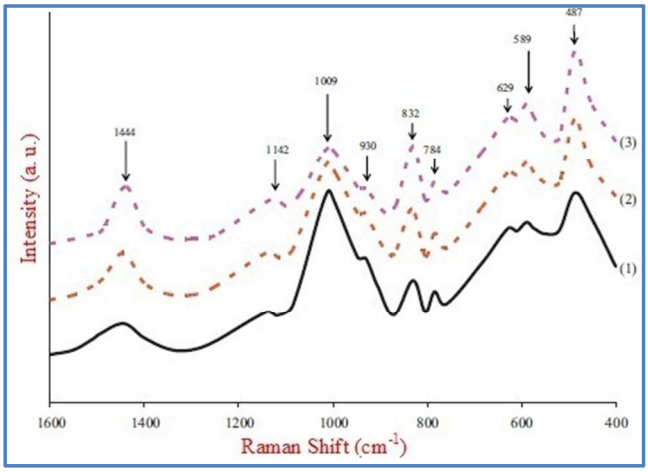

Fig. 21: Raman spectra of glass $40SrO\text{-}5Al_2O_3\text{-}15B_2O_3\text{-}40SiO_2$ irradiated with doses of (1) 0 kGy; (2) 10 kGy;and (3) 30 kGy [224]. (Reproduced with permission of Elsevier)

Table 8: Assignment of Raman bands in the spectra of Alumino-borosilicate glasses

Wave number (cm^{-1})	Raman assignments	Reference
1114	diborate groups	222
800 -1300	asymmetric vibration of SiO_4 tetrahedra	222
1000, 520	vibration of Si - O^-. B - O - B, B - O - Si and Si - O - Si bending	222
952	symmetric stretching of the P - O^- bonds	222
951	B - O - Si stretching vibration	222
885	pyroborate groups	222
770	symmetric breathing vibration of six-membered rings one BO_4 tetrahedron	222
590, 425	O -P - O bending modes of the orthophosphate PO_4^{3-} unit	222
447	bending or rocking vibrations of the B - O - Si linkages, B - O - B, B - O - Si and Si - O - Si	222

3.9 Tellurite Glasses

The Raman spectra of various tellurite glasses are shown in Fig. 22. In tellurite glasses, the tellurium oxide works as glass former. The tellurite oxide has mainly three basic structures, namely TeO_4 (trigonal bipyramid, tbp), TeO_3 (pyramid) and an intermediate with$TeO_{3+\delta}$ polyhedral. The four oxygen atoms are covalently bonded with central tellurium atom in TeO_4. The bipiramid structure is formed by two equatorial and two apex oxygen sites. The trigonal pyramid structure consisted of two bridging oxygen sites and one non-bridging oxygen atom [231-232]. The Raman bands near 667 cm^{-1} are related with combined vibrations of asymmetric stretching of $Te\text{–}_{eq}O_{ax}\text{–}Te$ bonds and symmetric stretching of TeO_4 tbps. The addition of Na_2O in glassy matrix changes the intensity of bands due to stretching vibrations of non-bridging $Te\text{–}O^-$ bonds in TeO_3 tps (753 and 792 cm^{-1}). The position of band assigned to the symmetric bending vibration of TeO_4 tbps is shifted towards low wavenumber side. The intense band at 40 cm^{-1} is associated with Boson peak. The increase of Na_2O content in tellurite glasses results the transformation of TeO_4 tbps to TeO_3 tps due to increased number of NBOs [233-234]. Assignment of main Raman bands in the spectra of tellurite glasses are listed in Table 9.

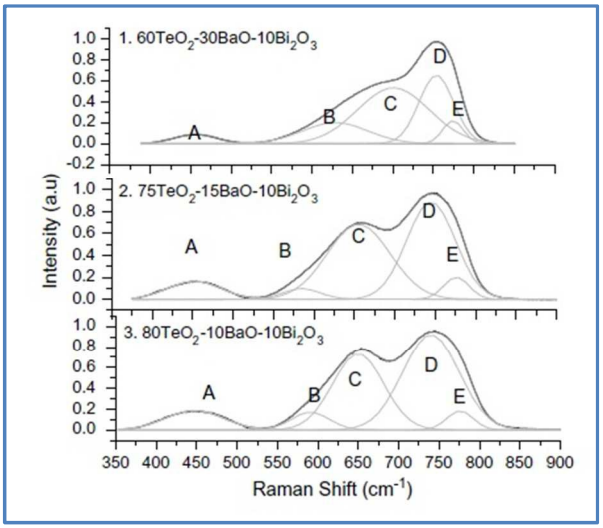

Fig. 22: Raman spectra of various tellurite glasses [231]. (Reproduced with permission of Elsevier)

Table 9: Assignment of main Raman bands in the spectra of tellurite glasses.

Wave number (cm^{-1})	Raman assignments	Reference
40	Boson peak	233-234
60-80	β-TeO_2	239
110-143	γ-TeO_2	239
300	TeO_3	236
440-478	stretching and bending vibration of Te–O–Te linkages in TeO_4 (tbp's), $TeO_{3+\delta}$ polyhedra and TeO_3 (tp's)	231, 235, 236, 243, 246
581-623	vibration of the continuous network comprised of TeO_4 tbp's	231
648-700	antisymmetric vibrations of Te–O–Te in $TeO_{3+\delta}$, TeO_4, TeO_3 and TeO_4 networks	231, 233-234, 239, 250
716-753	stretching vibrations between tellurium and non-bridging oxygen (NBO's) atoms	231, 233-234, 239, 250
773-793	continuous network vibration of TeO_4 tbp's and a TeO^- stretching vibration of $TeO_{3+\delta}$ polyhedra or TeO_3	231, 233-234, 239, 250

The study of $xNa_2O.(35\text{-}x)V_2O_5.65TeO_2$ glass showed the increase in intensities of TeO_4 tbp (443-478 cm^{-1} and 671-675 cm^{-1}) and TeO_3 tp (783-793 cm^{-1}) with increase of Na_2O content. This result is also consistent with above result of transformation of TeO_4 tbps to TeO_3 tps [235]. The network Te-O-Te bridges are breaked by addition network modifiers Na_2O, ZnO and ZnF_2 in tellurite and forms the non-bridging oxygens. The intensity of vibrations TeO_3 (300 cm^{-1}), Te-O-Te (470 cm^{-1})/TeO_4 (675 cm^{-1}) are reduced by replacement of ZnO with ZnF_2 in glassy matrix. The tellurium chain was breaked by introduction of P_2O_5 in tellurite glasses and suggests the formation of Te-O-P bonds [236]. Raman peaks of crystallized sodium tellurite glasses are very sharp and intense. The peak positions were shifted towards lower wavenumber side with increase of crystallization temperature [237]. The network of TeO_4 bypiramids are breaked to networks of TeO_{3+1} and TeO_3 polyhedra at high pressures [238]. Raman spectra of zinc tellurite glasses confirms the presence β-TeO_2 (60-80 cm^{-1}), γ-TeO_2 (110-143 cm^{-1}). The three dimension network of asymmetrical vibration of TeO_4 unit with one lone pair of electron at equilateral position is linked with Te_{ax}-O_{eq}-Te linkages. The formation of $Zn_2Te_3O_8$ units changes the bands positioned at 295, 343 and 700-800 cm^{-1} [239-241]. The peak positions of bands at 423 cm^{-1} is found to shift towards lower wave numbers with increasing ZnO content whereas bands at 661 and 720 cm^{-1} are shifted towards larger wavenumber side with increasing ZnO concentration. The intensities of bands at 661 cm^{-1} (decrease) and 720 cm^{-1} (increase) are reversed order with increase of ZnO content from 18 to 35 mol%. This indicates the decrease in Te–O coordination due to conversion of TeO_4 into TeO_3 structural units with increase of ZnO content [242]. Raman study of TeO_2–La_2O_3–TiO_2 glasses shows the chain formation of Te–O–Ti–O–Te– at lower content of TiO_2 whereas the chain formation becomes saturated and some TiO_4 polyhedron are also formed in glassy matrix [243]. The structural change from TeO_4 trigonal bipyramid (tbps) to TeO_3 trigonal pyramid (tps) via $[TeO_{3+1}]$ is also observed with increasing Ta_2O_5 content in glass [244]. The Raman spectra (89-x) TeO_2–$10TiO_2$–$1Nd_2O_3$–xWO_3 indicates a depolymerisation of tellurite glass as the Te–O–Te inter-chain linkages are progressively substituted by stronger Te–O–W bridges by the addition of WO_3 [245]. The addition of Nb_2O_5 in tellurite glasses decreases the connectivity by the deformation of Te–O–Te linkages [246]. The network modifying nature of K^+ ions is greater than that of Li^+ ions in the alkali metal tellurite glasses due to larger ionic radius of potassium than that of lithium [247]. The thallium ions in tellurite glasses induces the island-like structure of $[TeO_3]^{2-}$ [248]. The alkali ions (Li and Na) transports drive the secondary event as NBO migration through BO–NBO switching [249]. Khanna et al studied the Raman spectra of boro-tellurite and aluminoboro-tellurite glasses. Raman spectra of boro-tellurite glass depicts the bands at 450, 503, 615, 665, 718, 762, and 902 cm^{-1} whereas alumino-boro-tellurite glasses have Raman bands located at 337, 450, 505, 567, 606, 666, 724, 754 and 864 cm^{-1} [250]. The structural units TeO_4 tbp's and TeO_{3+1} polyhedra changes into TeO_3 tp's with an increase of B_2O_3 content [251]. The diamond in tellurite glasses is the good medium for quantum information. The first order diamond Raman band is assigned at 1350 cm^{-1} in nano-diamond induced tellurite glasses [252].

4. Conclusions

A detailed study of Raman spectroscopic data on alkali and alkaline earth metal doped various oxide glasses is reviewed. The various models were helpful for the truthful correlation of data. A general agreement was found that the structure of glassy network is compositional dependent. The vibrational properties of structural units are better understood in their structure and bonding as the vibrational spectroscopy cannot be useful as a tool for analyzing their detailed molecular structure. Raman spectroscopic studies of rectify the modification in vibration networks of borate by alkali and alkaline earth metals. The basic borate networks are formed by NBO and BO atoms in tetrahedral borate unit [9]. The formation of pentaborate, tetraborate, diborate, metaborate and pyroborate units [10], disappears of diborate units [102], boroxol ring [116] and high polymeric units such as pentaborate [105] by certain dopants was clearly noted by Raman spectroscopic studies of various borate glasses. It was found in Raman spectroscopy of oxide glasses that the modifying nature of alkali and alkaline metal are in the order of Cs < K < Na < Li < Ca < Mg [23]. The alkaline metals are effective in the order of Ba < Sr < Ca < Mg whereas the alkalis are in the order of K < Na < Li. The significant information glass forming ability of various glassy networks was obtained Raman spectroscopic studies in the present review article. On the basis of above investigations about oxide glasses, dopants MoO_3, CeO_2, Bi_2O_3, Sb_2O_3 and TeO_2 form mainly MoO_6 or MoO_4, CeO_8, BiO_3 or BiO_6, SbO_3 and TeO_3 or TeO_4 units, respectively. Raman study is also providing significant UV, β and ν-ray irradiations. It was found that these radiations decrease the Q^2_{Si} species in comparison to Q^3_{Si} and it reduces thee oxidation state of cations [230]. The tellurium oxide works as network former as well as network modifier. With the addition of alkali oxides, the TeO_4 tbps units transform into TeO_3 tps due to increased number of NBOs.

The great advances have been seen in the structural studies of glasses in past few decades still few open questions remain to study. The presence or absence of superstructural units in the glass network is the most important question. The mesounits in an intermediate- or medium-range order in the oxide structure are affecting a variety of the properties of the glass and are constituted by 7–20 or more atoms. The primary information about mesounits and their possible arrangements can be derived from the study of crystal structures isocompositional with the glasses. Such types of informations are questions for Raman spectroscopy. The quantitative information of structural units of glasses is a question for Raman spectroscopic analysis. It is always a question that informations obtained by Raman spectroscopy are either complete information or not. The vibrations, which are antisymmetrical with respect centre, are Raman inactive. In this case, it is a question that how can anti-symmetric vibrations be analysed by Raman spectroscopy. Such vibrations are analysed by infrared spectroscopy. What do the analogies with organic high polymers teach us for the glass? In what respect is given glass to be called a polymer?

The absence of change of P-coordination in phosphate glasses as found in borate are unanswered by structural study of phosphate glasses by Raman spectroscopy. There is no particular relationship seen between distribution of tetrahedral linkages and glass properties. A question is also arising that are there any

differences between the non-bridging oxygens on individual Q^2_P and Q^1_P tetrahedra.

Acknowledgements

Authors are thankful to the publishers Elsevier, Mineralogical Society of America, Springer, IOP science and EBSCO Publishing for giving permission for reproduction of cited contributions for academic purpose as review article. Authors acknowledge to the authors of cited articles. The funding agency CSIR, New Delhi, (India) is gratefully acknowledged for financial support under project No. 03(1300)/13/EMR-II.

References:

[1] L. Dussubieux, B. Gratuze and M. Blet-Lemarquand, *J. Archaeol Sci.,* 2010, **37**, 1646.
[2] A. Macfarlane and G. Martin, *Glass: A World History*. University of Chicago Press, 2002.
[3] R. K. Brow and M. L. Schmitt, *J. Euro. Ceram.Soc*., 2009, **29**,1193.
[4] B. Wei, H. Cao and S. Song, *Mater. Des.*, 2010, **31**, 4244.
[5] A. Goel, M. J. Pascual and J. M. F. Ferreira, *Int J Hydrogen Energy*, 2010, **35**, 6911.
[6] W. H. Zachariasen, *J. Am. Chem. Soc*., 1932, **54**, 3841.
[7] P. B. Price, L. M. Cook and A. Markar, *Nature*, 1987, **325**, 137.
[8] T. Lopez, E. Haro-Poniatowski, P. Bosh, M. Asomoza And R. Gomez, M. Massot and M. Balkanski, *J. Sol-Gel Science and Technology*, 1994, **2**, 891.
[9] Ch.-P. E. Varsamis, A. Vegiri and E. I. Kamitsos, *Cond. Matter Phys*, 2001, **4**, 119.
[10] K. S. Oo, M. Lwin, P. Kaung and S. Htoon, *J. Myan. Acad. Arts & Sc.*, 2006, **4**, 277.
[11] G. Padmaja and P. Kistaiah, *J. Phys. Chem. A*, 2009, **113**, 2397.
[12] N. C. A. de Souza, C. C. Santos, I. Guedes, N. O. Dantas and M. V. D. Vermelho, *Optical Mater*., 2013, **35**, 2544.
[13] Q. Chen, Q. Chen, S. Wang, *Open J. Inorg. Non-met. Mater*., 2011, **1**, 1.
[14] S. Bale and S. Rahman, *ISRN Spectroscopy*, 2012, **2012**, 1.
[15] Y. Wang, T. Honma and T. Komatsu, *J. Non-Cryst. Solids*, 2014, **383**, 86.
[16] P. McMillan, *Am. Mineralogist*, 1984, **69**, 622.
[17] P. F. McMillan and R. L. Remmele, Jr., *Am. Mineralogist*, 1986, **71**, 772.
[18] Y. Jinglin, J. Guochang, C. Hui and X. Kuangdi, *Rare Metals*, 2006, **25**, 431.
[19] R. P. Hapanowicz and R. A. Condrate, Sr., *J. Solid State Chem*., 1996, **123,** 183.
[20] M. Wang, J. CHeng, M. Li and F. He, *Physica B*, 2011, **406**, 3865.
[21] A. G. Kalampounias, *Bull. Mater. Sci*., 2011, **34**, 299.
[22] B. O. Mysen, L. W. Finger, D. Vigro and F. A. Seifert, *Am. Mineralogist*, 1982, **67**, 686.
[23] P. McMillan, *Am. Mineralogist*, 1984, **69**, 645459.
[24] L. D. Ferri, P. P. Lottici and G. Vezzalini, *Corrosion Sci.*, 2014, **80**, 434.
[25] H. Jia, G. Chen and W. Wang, *Optical Mater*., 2006, **29**, 445.
[26] H. Liu, J. Ma, J. Gong and J. Xu, *J. Non-Cryst. Solids*, 2015, **419**, 92.
[27] M. Karabulut, H. Ertap and M. Yüksek, *J. Non-Cryst. Solids*, 2015, **417**–**418**, 39.
[28] L. Ma, R. K. Brow, L. Ghussn and M. E. Schlesinger, *J. Non-Cryst. Solids*, 2015, **409**, 131.
[29] M. Farouk, *J. Non-Cryst. Solids*, 2014, **402**, 74.
[30] L. Song, J. Wu, Z. Li, X. Hao and Y. Yu, *J. Non-Cryst. Solids*, 2015, **419**, 16.
[31] P. Stoch and A. Stoch, *J. Non-Cryst. Solids*, 2015, **411**, 106.
[32] G. Pablo, Debenedetti and F. H. Stillinger, *Nature*, 2001, **410**, 259.
[33] M. Yamane and Y. Asahara, *Glasses for Photonics*, Cambridge University Press, Cambridge, 2000.
[34] A. L. Greer, *Nature*, 1999, **402**, 132.
[35] E. Axinte, *Materials and Design*, 2011, **32**, 1717.
[36] J. Schroers, *Nature*, 2014, **512**, 142.
[37] N. Karpukhina, R. G. Hilla and R. V. Law, *Chem. Soc. Rev*., 2014, **43**, 2174.
[38] G. W. Morey, *J. Industrial and Engineering Chemistry*, 1922, 823.
[39] J. Kieffer, *J. Phys. Chem. B*, 1999, **103**, 4153.
[40] A.K. Varshneya and J. C. Mauro, *European J. Glass Science and Technology Part A*, 2010, **51**, 28.
[41] L. Wondraczek, S. Sen, H. Behrens and R. E. Youngman, *Phys. Rev. B*, 2007, **76**, 014202.
[42] J.C. Mauro, D.C. Allan and M. Potuzak, *Phys. Rev. B*, 2009, **80**, 094204.
[43] J. C. Mauro and M. M. Smedskjaer, *J. Non-Cryst. Solids*, 2014, **396**–**397**, 41.
[44] J. E. Stanworth, *Nature*, 1952, **169**, 581.
[45] C. R. Gautam and A. K. Yadav, *ISRN Ceramics*, 2012, **2012**, 1.
[46] M. C. Eckersley, P. H. Gaskell, A. C. Barnes and P. Chieux, *Nature*, 1988, **335**, 525.
[47] S. Singh, M. D. Ediger and J. J. de Pablo, *Nature Materials*, 2013, **12**, 139.
[48] Zhong-Hong Jiang and Qin-Yuan Zhang, *Prog. Mater. Sci.*, 2014, **61**,144.
[49] M. Poulain, *Nature*, 1981, **293**, 279.
[50] A. Fluegel, *Glass Technol: Eur J Glass Sci Technol A*, 2007, **48**, 13.
[51] A. K. Yadav and C. R. Gautam, *Adv. Appl. Ceram*., 2014, **113**, 193.
[52] A. K. Yadav and C. R. Gautam, *Spectroscopy Lett*., 2015, **48**, 514.
[53] A. K. Yadav and C. R. Gautam, *Adv.Appl. Ceram*., 2014, **113**, 193.
[54] M. Yamane and Y. Asahara, Glasses for photonics, Cambridge University, Cambridge, UK, 2000.
[55] J. C. Phillips and M. F. Thorpe, *Solid State Commun*. 1985, **53**, 699.
[56] P. K. Gupta and J. C. Mauro, *The Journal of Chemical Physics*, 2009, **130**, 094503.
[57] P. G. Pavani, K. Sadhana and V. C. Mouli, *Physica B*, 2011, **406**, 1242.
[58] K. Cho, J. Oh, T. Lee and D. Shin, *J. Power Sources,* 2008, **183**, 431.
[59] S. Baccaro, N. Catallo, A. Cemmi and G. Sharma, *Nuclear Instr. & Meth. Phys. Res. Section B-Beam Interactions with Mater. and Atoms*, 2011, **269**, 167.
[60] Y. J. Chen, X. H. Gong, Y. F. Lin, Z. D. Luo and Y. D. Huang, *Optical Materials*, 2010, **33,** 71.
[61] S. P. Singh, R. P. S. Chakradhara, J. L. Rao and B. Karmakar, *J. Alloys and Comp.,* 2010, **493**, 256.
[62] R. Gehring, *Scientific American Inc*, 1890, **737**, 11776.
[63] R. Dupree, D. Holland and M.G. Mortuza, *Nature*, 1987, **328**, 416.
[64] L. Cormier, G. Calas and B. Beuneu, *J. Non-Cryst. Solids*, 2011, **357**, 926.
[65] A. M. Efimov, *J. Non-Cryst. Solids*, 1999, **253**, 95.
[66] E. M. Rabinovich, *J. Mater. Sci.*, 1976, **11**, 925.
[67] M. Karabulut, E. Melnik, R. Stefan, G. K. Marasinghe, C. S. Ray, C. R. Kurkjin and D. E. Day, *J. Non-Cryst. Solids*, 2001, **288**, 8,.
[68] K. El-Egili, H. Doweidar, Y. M. Moustafa and I. Abbas, *Physica B*, 2003, **339**, 237.
[69] G. Guimbretière, D. Bégué, M. Dussauze and V. Rodriguez, *Vibrational Spect*., 2012, **63**, 426.
[70] P.B. Price, L.M. Cook and A. Marker, Nature, 1987, **325**, 137.
[71] A. A. Osipov, L. M. Osipova and V. E. Eremyashev, *Glass Phys. Chem*., 2013, **39**, 105.
[72] O. N. Koroleva, L. A. Shabunina and V. N. Bykov, *Glass and Ceramics*, 2011, **67**, 340.
[73] A. Goel, J. S. McCloy, C. F. W. Jr, B. J. Riley, M. J. Schweiger and C. P. Rodriguez and J. M. F. Ferreira, *Int. J. Appl. Glass Sci.*, 2012, 1.
[74] J. Blizard, *Industrial and Engineering Chemistry*, 1947, **39**, 1215.
[75] L. Koudelka, P. Mosner and J. Šubčík, *IOP Conf. Ser.: Mater. Sci. Eng*. 2009, **2**, 012015.
[76] D. Kim, C. Hwang, D. Gwoo, T. Kim, N. Kim and B.-K. Ryu, *Electr. Mater. Lett.*, 2011, **7**, 343.
[77] A. Naumaan and J. T. Boyd, *J. Electrochem. Soc.*, 1980, **127**, 1414.
[78] A. Tilocca, *Phys. Rev. B*, 2007, **76**, 224202.
[79] S. W. Lee, K. S. Ryoo, J. E. Kim, J. H. Lee, C. D. Kim and K. S. Hong, *J. Mater. Sci.*, 1994, **29**, 4577.

[80] J. L. Rygel, Y. Chen, C. G. Pantano, T. Shibata, J. Du, L. Kokou, R. Woodman and J. Belcher, *J. Am. Ceram. Soc.*, 2011, **94**, 2442.

[81] R. W. Cahn, *Nature*, 1989, **341**, 183.

[82] M. Handke, M. Sitarz, M. Rokita and E. Galuskin, *J. Molecular Struc.*, 2003, **651**, 39.

[83] L. Cormier and D. R. Neuville, *Chem. Geo*., 2004, **213**, 103.

[84] S. L. S. Rao, G. Ramadevudu, Md. Shareefuddin, A. Hameed, M. N. Chary and M. L. Rao, *Int. J. Eng., Sci. Tech*., 2012, **4**, 25.

[85] D. P. Singh and G. P. Singh, *J. Alloys Comp*., 2013, **546**, 224.

[86] G. Calas, L. Cormier, L. Galoisy and P. Jollivet, *C. R. Chimie*, 2002, **5**, 831.

[87] J. Qiu, X. Jiang, C. Zhu, H. Inouye, J. Si and K. Hirao, *Opt Lett.*, 2004, **29**, 370.

[88] Q. Yu, F. Chen, T. Xu, S. Dai and Q. Zhang, *J. Non-Cryst. Solids*, 2013, **378**, 254.

[89] M. Diem (Ed.), *Introduction to Modern Vibrational Spectroscopy*, New York: Wiley-Interscience, 1993.

[90] C. V. Raman and K. S. Kirishnan, *Nature*, 1928, **121**, 501.

[91] C. V. Raman, *Indian J. Phys*., 1928, **2**, 387-398.

[92] C. C. Lin, M. T. Kuo and H. C. Chang, *J. Med. Biolog. Engg.*, 2010, **30**, 343-354.

[93] C. V. Raman and K. S. Krishnan, *Indian J. Phys*., 1928, **2**, 399.

[94] C. V. Raman, K. S. Krishnan, *Nature (London)*, 1928, **121**, 619.

[95] L. A. Lyon, C. D. Keating, A. P. Fox, B. E. Baker, H. Lin, S. R. Nicewarner, S. P. Mulvaney and M. J. Natan, *Analytical Chemistry*, 1998, **70**, 341R.

[96] H. H. Willard, Jr. L. L. Merritt and J. A. Dean, Raman Spectroscopy. In Instrumental Methods of Analysis, 5th ed, D. Van Nostrand Co., New York, 1974 ,189.

[97] B. H. Stuart, Infrared Spectroscopy, Fundamentals and Applications. J. Wiley, Chichester, West Essex, England, 2004, 2.

[98] M. S. Shackley, X-Ray Fluorescence Spectrometry (XRF) in Geoarchaeology. Springer, New York, 2010, 16

[99] T. Lopez, E. H. Poniatowski, P. Bosh, M. Asomoza, R. Gomez, M. Massot and M. Balkanski, *J. Sol-Gel Sci. Tech.*, 1994, **2**, 891.

[100] M. Loubser, *Chemical and Physical Aspects of Lithium Borate Fusion*, Distertation M. Sc. University of Pretoria, Pretoria, 2009.

[101] W. Di, W. Song-ming, Z. Qing-li, S. Dun-lu, Y. Shao-tang, Y. Jing-lin and W. Yuan-yuan, *Chin. J. Quan. Elect.*, 2011, **28**, 241.

[102] M. Ganguli and K. J. Rao, *J. Solid State Chem.,* 1999, **145**, 65.

[103] G. Padmaja and P. Kistaiah, *J. Phys. Chem. A*, 2009, **113**, 2397.

[104] T. Yano, N. Kunimine, S. Shibata and M. Yamane, *J. Non-Cryst. Solids*, 2003, **321**, 137.

[105] Q. Jiao, X. Yu, X. Xu, D. Zhou and J. Qiu, *J. Solid State Chem.*, 2013, **202**, 65.

[106] A. A. A. Shama and F. H. El-Batal, *Egypt. J. Solids*, 2006, **29**, 49.

[107] M. Affatigato, S. Feller, A. K. Schue, S. Blair, D. Stentz, G. B. Smith, D. Liss, M. J Kelley, C. Goater and R. Leelesagar, *J. Phys.: Condens. Matter*, 2003, **15**, S2323.

[108] Q. Chen, Q. Chen, S. Wang, *Open J. Inorg. Non-met. Mater.*, 2011, **1**, 1.

[109] V. Timar, R. Lucăcel-Ciceo and I. Ardelean, *Quan. Electr. Optoelectronics*, 2008, **11**, 221.

[110] J. Schwarz and H. Tichá, *J. Optoelectr. Adv. Mater.*, 2003, **5**, 69.

[111] A. A. Alemi, H. Sedghi, A. R. Mirmohseni and V. Golsanamlu, *Bull. Mater. Sci.*, 2006, **29**, 55.

[112] A. Toderas, M. Toderas, S. Filip and I. Ardelean, *Optoelectr. Adv. Mater. Rapid Comm.,* 2012, **6**, 331.

[113] B. S. Cristian, *Study of some structural and physical properties of some B_2O_3 based glasses containing Ag_2O and 3d ions,* Ph.D. thesis, Babeş-Bolyai University, 2011.

[114] S. C. Baidoc and I. Ardelean, *J. Optoelectr. Adv. Mater.*, 2008, **10**, 3205.

[115] R. Uning, W. M. Hua and R. Hussin, *Structural studies of strontium borate glass doped with Zn^{2+}, Mn^{2+} and Fe^{2+} ions*, UMTAS 2011.

[116] S.R. Rejisha, P.S. Anjana, N. Gopakumar and N. Santha, *J. Non-Cryst. Solids*, 2014, **388**, 68.

[117] M. Bettinelli, A. Speghini, M. Ferrari and M. Montagna, *J. Non-Cryst. Solids*, 1996, **201**, 211.

[118] S. Suresh, M. Prasad, G Upender, V. Kamalaker and V. C. Mouli, *Ind. J. Pure and Appl. Phys*., 2009, **47**, 163.

[119] D. Maniu, I. Ardelean, T. Iliescu, S. Cınta, V. Nagel and W. Kiefer, *J. Molecular Struct*., 1999, **480**, 657.

[120] D. Maniu, T. Iliescu, I. Ardelean, S. Cinta-Pinzaru, N. Tarcea and W. Kiefer, *J. Molecular Struct*., 2003, **651**, 485.

[121] C. N. Santos, D. D. S. Meneses, P. Echegut, D. R. Neuville, A. C. Hernandes and A. Ibanez, *Appl. Phys. Lett*., 2009, **94**, 151901.

[122] R. S. Barker, D. A. Richardson, E. A. G. Mcconkey and R. Rimmer, *Nature*, 1960, **187**, 135.

[123] B. Tiwari, A. Dixit, G. P. Kothiyal, M. Pandey and S. K. Deb, *Preparation and characterization of phosphate glasses containing titanium*, National Symposium on Science & Technology of Glass and Glass-Ceramics (NSGC-06) held during September 15-16, at BARC, Mumbai, 2006,

[124] L. F. Santos, R. M. Aldeida, V. K. Tikhomirov and A. Jha, *J. Non-Cryst. Solids*, 2001, **284**, 43.

[125] A. Mogus-Milankovic, A. Gajovic, A. Santic and D. E. Day, *J. Non-Cryst. Solids*, 2001, **289**, 204.

[126] K. Brahmachary, D. Rajesh, S. Babu and Y. C. Ratnakaram, *J. Molecular Struct.* 2014, **1064**, 6.

[127] A. Kiani, J. V. Hanna, S. P. King, G. J. Rees, M. E. Smith, N. Roohpour, V. Salih and J. C. Knowles, *Acta Biomaterialia*, 2012, **8**, 333.

[128] M. Elisa, I. C. Vasiliu, C. E. A. Grigorescu, B. Grigoras, H. Niciu, D. Niciu, A. Meghea, N. Iftimie, M. Giurginca, H. J. Trodahl and M. Dalley, *Optical Mater*., 2006, **28**, 621.

[129] F. H. El-Batal, *Ind. J. Pure and Appl. Phys*., 2009, **47**, 631.

[130] D. Toloman, R. Ciceo-Lucacel, D. A. Magdas, A. Regos, A. R. Biris, C. Leostean, I. Ardelean, *J. Alloys Comp.*, 2013, **556**, 67.

[131] B. Qian, X. Liang, C. Wang and S. Yang, *J. Nuclear Mater*., 2013, **443**, 140.

[132] C. I. R. D. Oliveira, L. F. C. D. Oliveira, F. A. D. Filho, Y. Messaddeq and S. J. L. Ribeiro, *Spectrochimica Acta Part A*, 2005, **61**, 2023.

[133] D. Ilieva, B. Jivov, G. Bogachev, C. Petkov, I. Penkov and Y. Dimitriev, *J. Non-Cryst. Solids*, 2001, **283**, 195.

[134] D. Ilieva, B. Jivov, D. Kovacheva, Ts. Tsacheva, Y. Dimitriev, G. Bogachev and C. Petkov, *J. Non-Cryst. Solids*, 2001, **293-295**, 562.

[135] L. Koudelka, I. Rösslerová, J. Holubová, P. Mošner, L. Montagne and B. Revel, *J. Non-Cryst. Solids*, 2011, **357**, 2816.

[136] G. L. Flower, M. S. Reddy, G. S. Baskaran and N. Veeraiah, *Optical Mater*., 2007, **30**, 357.

[137] S. S. Sastry and B. R. V. Rao, *Physica B*, 2014, **434**, 159.

[138] G. Le Saout, F. Fayon, C. Bessada, P. Simon, Annie Blin and Y. Vaills, *J. Non-Cryst. Solids*, 2001, **293-295**, 657.

[139] W. A. Pisarski, L. Zur, T. Goryczka, M. Sołtys and J. Pisarska, *J. Alloys Comp.*, 2014, **587**, 90.

[140] A. M. Milankovic, A. Santic, S. T. Reis, K. Furic and D. E. Day, *J. Non-Cryst. Solids*, 2005, **351**, 3246.

[141] G. S. Baskaran, G. L. Flower, D. K. Rao and N. Veeraiah, *J. Alloys Comp*., 2007, **431**, 303.

[142] A. Šantić, Ž. Skoko, A. Gajović, S. T. Reis, D. E. Day and A. M. Milanković, *J. Non-Cryst. Solids*, 2011, **357**, 3578.

[143] A. Santic, A. M. Milankovic, K. Furic, V. Bermanec, C. W. Kim and D. E. Day, *J. Non-Cryst. Solids*, 2007, **353**, 1070.

[144] A. M. Milankovic, A. Santic, A. Gajovic and D. E. Day, *J. Non-Cryst. Solids*, 2003, **325**, 76.

[145] B. Qian, X. Liang, S. Yang, S. He and L. Gao, *J. Molecular Struct.*, (2012)**1027**, 31.

[146] K. Joseph, M. Premila, G. Amarendra, K. V. G. Kutty, C. S. Sundar and P. R. V. Rao, *J. Nuclear Mater.*, 2012, **420**, 49.

[147] Y. M. Lai, X. F. Liang, S. Y. Yang, J. X. Wang, L. H. Cao and B. Dai, *J. Molecular Struct.*, 2011, **992**, 84.

[148] Y. M. Lai, X. F. Liang, S. Y. Yang, J. X. Wang and B. T. Zhang, *J. Molecular Struct.*, 2012, **1013**, 134.

[149] S. Chakraborty and A. K. Arora, *Vibrational Spectr.*, 2012, **61**, 99.

[150] P. S. Rao, P. M. V. Teja, A. R. Babu, C. Rajyasree and D. K. Rao, *J. Non-Cryst. Solids*, 2012, **358**, 3372.

[151] N. Kitamura, K. Fukumi, J. Nakamura, T. Hidaka, T. Ikeda, H. Hashima and J. Nishii, *J. Non-Cryst. Solids*, 2011, **357**, 1188.

[152] P. S. Rao, S. B. M. Krishna, S. Yusub, P. R. Babu, C. Tirupataiah and D. K. Rao, *J. Molecular Struct.*, 2013, **1036**, 452.

[153] S. Thomas, R. George, M. Rathaiah, V. Venkatramu, S. N. Rasool and N. V. Unnikrishnan, *Physica B*, 2013, **431**, 69.

[154] S. H. Santagneli, G. Poirier, M. T. Rinke, S. J. L. Ribeiro, Y. Messaddeq and H. Eckert, *J. Non-Cryst. Solids*, 2011, **357**, 2126.

[155] R. C. Lucacel, A. O. Hulpus, V. Simonn and I. Ardelean, *J. Non-Cryst. Solids*, 2009, **355**, 425.

[156] A. M. B. Silva, R. N. Correia, J. M. M. Oliveira and M. H. V. Fernandes, *J. Euro. Ceram. Soc.*, 2010, **30**, 1253.

[157] I. D. F. Gimenez, I. O. Mazali and O. L. Alves, *J. Phys. Chem. Solids*, 2001, **62**, 1251.

[158] S. N. Rasool, L. R. Moorthy and C. K. Jayasankar, *Optics Comm*., 2013, **311** 156.

[159] M. Elisa, B. A. Sava, I. C. Vasiliu, R. C. C. Monteiro, J. P. Veiga, L. Ghervase, I. Feraru and R. Iordanescu, *J. Non-Cryst. Solids*, 2013, **369**, 55.

[160] N. Vedeanu, O. Cozar, I. Ardelean, B. Lendl and D. A. Magdas, *Vibrational Spectr*., 2008, **48**, 259.

[161] A. Chahine, M. Et-tabirou and J. L. Pascal, *Mater. Lett*., 2004, **58**, 2776.

[162] E. Metwalli, M. Karabulut, D. L. Sidebottom, M. M. Morsi and R. K. Brow, *J. Non-Cryst. Solids*, 2004, **344**, 128.

[163] N. Kerkouri, M. Haddad, M. Et-Tabirou, A. Chahine and L. Laanab, *Physica B*, 2011, **406**, 3142.

[164] C. Ivascu, I. B. Cozar, L. Daraban and G. Damian, *J. Non-Cryst. Solids*, 2013, **359**, 60.

[165] C. Ivascu, A. Timar Gabor, O. Cozar, L. Daraban and I. Ardelean, *J. Molecular Struct*., 2011, **993**, 249.

[166] S. Hraiech, M. Ferid, Y. Guyot and G. Boulon, *J. Rare Earths*, 2013, **31**, 685.

[167] B. G. Parkinson, D. Holland, M. E. Smith, C. Larson, J. Doerr, M. Affatigato, S. A. Feller, A. P. Howes and C. R. Scales, *J. Non-Cryst. Solids*, 2008, **354**, 1936.

[168] D. Manara, A. Grandjean and D. R. Neuville, *Am. Mineralogist*, 2009, **94**, 777.

[169] M. Lenoir, A. Grandjean, S. Poissonnet and D. R. Neuville, *J. Non-Cryst. Solids*, 2009, **355**, 1468.

[170] M. Lenoir, A. Grandjean, Y. Linard, B. Cochain and D. R. Neuville, *Chem. Geo.*, 2008, **256**, 316.

[171] M. Jroda and C. Paluszkiewicz, *J. Molecular Struct.*, 2007, **834–836**, 302.

[172] V. E. Eremyashev, A. A. Osipov and L. M. Osipov, *Glass and Ceramics*, 2011, **68**, 205.

[173] A. Winterstein-Beckmann, D. Möncke, D. Palles, E. I. Kamitsos and L. Wondraczek, *J. Non-Cryst. Solids*, 2014, **401**, 110.

[174] H. Yamashita, K. Nagata, H. Yoshino, K. Ono and T. Maekawa, *J. Non-Cryst. Solids*, 1999, **248**, 115.

[175] D. Chen, H. Miyoshi, H. Masui, T. Akai and T. Yazawa, *J. Non-Cryst. Solids*, 2004, **345-346**, 104.

[176] D. A. McKeown, I. S. Muller, Hao Gan, I. L. Pegg and C. A. Kendziora, *J. Non-Cryst. Solids*, 2001, **288**, 191.

[177] D. A. McKeown, I. S. Muller, H. Gan, I. L. Pegg and W. C. Stolte, *J. Non-Cryst. Solids*, 2004, **333**, 74.

[178] X. Zhang, Y. Wang, J. Lu, J. Zang, J. Zhang, E. Ge, *Int. Journal of Refractory Metals & Hard Mater*., 2010, **28**, 260.

[179] D. A. McKeown, I. S. Muller, A. C. Buechele, I. L. Pegg and C. A. Kendziora, *J. Non-Cryst. Solids*, 2000, **262**, 126.

[180] T. G. V. M. Rao, A. R. Kumar, K. Neeraja, N. Veeraiah and M. R. Reddy, *J. Alloys Comp*., 2013, **557**, 209.

[181] Z. Wang, Q. Shu and K. Chou, ISIJ International, 2011, **51**, 1021.

[182] L. Rezazadeh, S. Baghshahi, A. Nozad Golikand and Z. Hamnabard, *Ionics*, 2013, 1.

[183] A. K. Yadav, C. R. Gautam, A. Gautam, V. K. Mishra, *Phase Transitions*, 2013, **86**, 1000.

[184] A. K. Yadav and C. R. Gautam, Optics & Photonics Journal, 2013, **3**, 1.

[185] C. R. Gautam, A. K. Yadav, V. K. Mishra and K. Vikram, *Open J. Non-met. Mater*., 2012, **2**, 47

[186] G. Kaur, O. P. Pandey, K. Singh, *J. Non-Cryst. Solids*, 2012, **358**, 2589.

[177] C. R. Gautam, A. K. Singh and A. K. Yadav, *Int. J. Appl. Natural Sci.*, 2012, **1**, 69.

[188] G. F. Zhang, T. S. Wang, K. J. Yang, L. Chen, L. M. Zhang, H. B. Peng, W. Yuan and F. Tian, *Nuclear Instr. Meth. Phys. Res. B*, 2013, **316**, 218.

[189] C. Gejke, E. Zanghellini, J. Swenson and L. Borjesson, *J. Power Sources*, 2003, **119–121**, 576.

[190] P. Mošner, M. Vorokhta, L. Koudelka, L. Montagne, B. Revel, K. Sklepić and A. M. Milanković, *J. Non-Cryst. Solids*, 2013, **375**, 1.

[191] N. Sdiri, H. Elhouichet and M. Ferid, *J. Non-Cryst. Solids*, 2014, **389**, 38.

[192] K. J. Rao, K. C. Sobha and S. Kumar, *Proc. Indian Acad. Sci. (Chem. Sci.)*, 2001, **113**, 497.

[193] A. Saranti, I. Koutselas and M. A. Karakassides, *J. Non-Cryst. Solids*, 2006, **352**, 390.

[194] L. Koudelka, J. Pospisil, P. Mosner, L. Montagne and L. Delevoye, *J. Non-Cryst. Solids*, 2008, **354**, 129.

[195] L. Koudelka, P. Mosner, M. Zeyer and C. Jager, *J. Non-Cryst. Solids*, 2003, **326-327**, 72.

[196] L. Koudelka, I. Rösslerová, Z. Černošek, P. Mošner, L. Montagne and B. Revel, *J. Non-Cryst. Solids*, 2014, **401**, 124.

[197] L. Koudelka and P. Mosner, *Mater. Lett.*, 2000, **42**, 194.

[198] L. Koudelka, P. Mosnera, J. Pospisila, L. Montagne and G. Palavit, *J. Solid State Chem*., 2005, **178**,1837.

[199] L. Koudelka, J. Subcik, P. Mosner, L. Montagne and L. Delevoye, *J. Non-Cryst. Solids*, 2007, **353**, 1828.

[200] J. Šubcík, L. Koudelka, P. Mošner, L. Montagne, B. Revel and I. Gregora, *J. Non-Cryst. Solids*, 2009, **355**, 970.

[201] P. Mosner, K. Vosejpková, L. Koudelka, L. Montagne and B. Revel, *Mater. Chem. Phys*. 2010, **124**, 732.

[202] K. Vosejpkova, L. Koudelka, Z. Cernosek, P. Mosner, L. Montagne and B. Revel, *J. Phys. Chem. of Solids*, 2012, **73**, 324.

[203] S. Petrescu, M. Constantinescu, E. M. Anghel, I. Atkinson, M. Olteanu and M. Zaharescu, *J. Non-Cryst. Solids*, 2012, **358**, 3280.

[204] C. L. Losq, D. R. Neuville, P. Florian, G. S. Henderson and D. Massiot, *Geochimica et Cosmochimica Acta*, 2014, **126**, 495.

[205] D. A. McKeown, F. L. Galeener and G. E. Brown Jr, *J. Non-Cryst. Solids*, 1984, **68**, 361.

[206] M. Okuno, N. Zotov, M. Schmucker, H. Schneider, *J. Non-Cryst. Solids*, 2005, **351**, 1032.

[207] P. McMillan, B. Piriou and A. Navrotsky, *Geochimica et Cosmochimica Acta*, 1982, **46**, 2021.

[208] P. McMillan and B. Piriou, *J. Non-Cryst. Solids*, 1983, **55**, 221.

[209] D. R. Neuville, L. Cormier and D. Massiot, *Geochimica et Cosmochimica Acta*, 2004, **68**, 5071.

[210] D. R. Neuville, L. Cormier and D. Massiot, *Chem. Geo*., 2006, **229**, 173.

[211] D. R. Neuville, L. Cormier, A. M. Flank, V. Briois and D. Massiot, *Chem. Geo*. 2004, **213**, 153.

[212] M. Licheron, V. Montouillout, F. Millot and D. R. Neuville, *J. Non-Cryst. Solids*, 2011, **357**, 2796.

[213] C. Huang and E. C. Behrman, *J. Non-Cryst. Solids*, 1991, **128**, 310.

[214] J. F. Stebbins, E. V. Dubinsky, K. Kanehashi and K. E. Kelsey, *Geochimica et Cosmochimica Acta*, 2008, **72**, 910.

[215] V. G. Plotnichenko, V. O. Sokolov, V. V. Koltashev and E. M. Dianov, *J. Non-Cryst. Solids*, 2002, **306**, 209.

[216] A. Trukhin and B. Capoen, *J. Non-Cryst. Solids*, 2005, **351**, 3640.

[217] S. Agathopoulos, D. U. Tulyaganov, J. M. G. Ventura, S. Kannan, A. Saranti, M. A. Karakassides and J. M. F. Ferreira, *J. Non-Cryst. Solids*, 2006. **352**, 322.

[218] H. Aguiar, E. L. Solla, J. Serra, P. González, B. León, F. Malz and C. Jäger, *J. Non-Cryst. Solids*, 2008, **354**, 5004.

[219] H. Aguiar, J. Serra, P. González and B. León, *J. Non-Cryst. Solids*, 2009, **355**, 475.

[220] A. Vulpoi, L. Baia, S. Simon, V. Simon, *Mater. Sci. Eng. C*, 2012, **32**, 178.

[221] Y. Gandhi, M. V. R.C. Rao, C. S. Rao, I. V. Kityk and N. Veeraiah, *J. Luminescence*, 2011, **131**, 1443.

[222] K. Cheng, J. Wan and K. Liang, *Mater. Lett.*, 2001, **47**, 1.

[223] H. Li, Y. Su, L. Li and D. M. Strachan, *J. Non-Cryst. Solids*, 2001, **292**, 167.

[224] A. R. Kumar, T. G. V. M. Rao, K. Neeraja, M. R. Reddy and N. Veeraiah, *Vibrational Spectr*., 2013, **69**, 49.
[225] E. Malchukova, B. Boizot, G. Petite and D. Ghaleb, *J. Non-Cryst. Solids*, 2008, **354**, 3592.
[226] E. Malchukova and B. Boizot, *Phys. Solid State*, 2008, **50**, 1687.
[227] E. Malchukova, B. Boizot, G. Petite and D. Ghaleb, *The Eur. Phys. J. Appl. Phys*., 2009, **45**, 10701.
[228] E. Malchukova, B. Boizot, D. Ghaleb and G. Petite, *J. Non-Cryst. Solids*, 2006, **352**, 297.
[229] E. Malchukova, B. Boizot, G. Petite and D. Ghaleb, *J. Non-Cryst. Solids*, 2007, **353**, 2397.
[230] E. Malchukovaa, B. Boizot, D. Ghaleb, G. Petite, *Nuclear Instr. Meth. Phys. Res. A*, 2005, **537**, 411
[231] A. jha, B. Richards, G. Jose, T. T. Fernandez, P. Joshi, X. Jiang and J. Lousteau, *Progress mater. sci.*, 2012, **57**, 1426.
[232] F. Pietrucci, S. Caravati and M. Bernasconi, *Phys. Rev. B*, 2008, **78**, 064203.
[233] A. Santic, A. M. Milankovic, K. Furic, M. R. Linaric, C. S. Ray and D. E. Dayd, *Croatica Chemica Acta*, 2008, **81**, 559.
[234] J. Heo, D. Lam, G. H. Sigel, Jr. E. A. Mendoza and D. A. Hensley, *J. Am. Ceram. Soc*., 1992, **75**, 277.
[235] M.M. Umair and A. K. Yahya, *Mater. Chem. Phys.*, 2013, **142**, 549.
[236] M. Irannejad, G. Jose, A. Jha and P. Steenson, *Optics Communications*, 2012, **285**, 2646.
[237] A. Jha, P. Joshi and S. Shen, *Optics Express*, 2008, **16**, 13526.
[238] E. Stavrou, C. Raptis and K. Syassen, *Phys. Rev. B*, 2010, **81**, 174202.
[239] D. Dutta, M. P. F. Graca, M. A. Valente and S.K. mendiratta, *Solid state ionics*, 2013, **230**, 66.
[240] M. Ceriotti, F. Pietrucci and M. Bernasconi, *Phys. Rev. B*, 2006, **73**, 104304-1 - 104304,.
[241] S. Manning, H. Ebendorff-Heidepriem and Tanya M. Monro, *Optical Mat. Express*, 2012, **2**, 140.
[242] A. Kaur, A. Khanna, C. Pesquera, F. González and V. Sathe, J. Non-Cryst. Solids, 2010, **356,** 864.
[243] W. Stambouli, H. Elhouichet and M. Ferid, *J. Molecular Structure*, 2012, **1028**, 39.
[244] I. Yakine, A. Chagraoui, A. Moussaoui and A. Tairi, *J. Mater. Environ. Sci.*, 2012, 3, 776.
[245] Hssen Fares, Ifa Jlassi, Habib Elhouichet and Mokhtar Férid, *J. Non-Cryst. Solids*, 2014, **396–397**, 1.
[246] A. Kaur, A. Khanna, V. G. Sathe, F. Gonzalez and B. Ortiz, *Phase Transitions*, 2013, 86, 598.
[247] R. Akagi, K. Handa, N. Ohtori, A.C. Hannon, M. Tatsumisago and N. Umesaki, *J. Non-Cryst. Solids*, 1999, **256 & 257**, 111.
[248] T. Hayakawa, M. Koduka, M. Nogami, J. R. Duclere, A. P. Mirgorodsky and P. Thomas, *Scripta Materialia*, 2010, **62**, 806.
[249] M. H. Bhat, M. Ganguli and K. J. Rao, *Current Science*, 2004, **86**, 676.
[250] N.Kaur and A. Khanna, *J. Non-Cryst. solids*, 2014, **404**, 116.
[251] P. Damas, J. Coelho, G. Hungerford and N. S. Hussain, *Mater. Res. Bull.*, 2012, **47**, 3489.
[252] M. R. Henderson, B. C. Gibson, H. Ebendorff-Heidepriem, K. Kuan, S. Afshar V., J. O. Orwa, I. Aharonovich , S. Tomljenovic-Hanic, A. D. Greentree, S. Prawer and T. M. Monro, *Adv. Mater*., 2011, **23**, 2806.
[253] M. M. Smedskjaer, J. C. Mauro, S. Sen and Y. Yue, *Chem. Mater*. 2010, **22**, 5358.